

## Evolution of Late Oligocene - Early Miocene attached and isolated carbonate platforms in a volcanic ridge context (Maldives type), Yadana field, offshore Myanmar

Paumard Victorien<sup>1,2,\*</sup>, Zuckmeyer Eric<sup>2,5</sup>, Boichard Robert<sup>2</sup>, Jorry Stephan<sup>3</sup>, Bourget Julien<sup>1</sup>, Borgomano Jean<sup>2,4</sup>, Maurin Thomas<sup>2</sup>, Ferry Jean-Noël<sup>2</sup>

<sup>1</sup> Centre for Energy Geoscience, School of Earth and Environment, University of Western Australia, 35 Stirling Highway, Crawley, WA 6009, Australia

<sup>2</sup> TOTAL Exploration and Production, CSTJF, Avenue Larribau, 64000, Pau, France

<sup>3</sup> IFREMER, Institut Carnot Edrome, Unité Géosciences Marines, Laboratoire Géodynamique et Enregistrements Sédimentaires, 29280 Plouzané, France

<sup>4</sup> Aix-Marseille Université, CNRS, IRD, CEREGE UM34, B.P. 80, 13545 Aix-en-Provence, France

<sup>5</sup> TOTAL Exploration and Production Asia Pacific, Odeon Towers, 188720 Singapore

\* Corresponding author : Victorien Paumard, email address : [victorien.paumard@research.uwa.edu.au](mailto:victorien.paumard@research.uwa.edu.au)

### Abstract :

This study investigates the stratigraphic evolution of the Late Oligocene - Early Miocene carbonate platforms of the Yadana area (offshore Myanmar). Well data, regional 2D and local 3D seismic surveys allow the identification of three shallow-water carbonate platforms (Yadana, 3DF and 3DE) showing various morphologic and stratigraphic patterns influenced by the presence of a paleohigh. The identification of seven seismic sequences in the Yadana area constrains the stratigraphic evolution in three stages: (1) development of aggrading attached and isolated platforms during the Chattian; (2) a period of platform emersion during the Oligocene - Miocene transition; (3) drowning of the smaller buildup (3DE) associated with km-scale backstepping on the large platforms (3DF and Yadana) during the Aquitanian. The Aquitanian marks the onset of renewed volcanic activity associated with the development of fringing carbonate reefs during the Burdigalian. The rapid (~6 My) development of these wide (~5–70 km) and thick (~300–850 m) carbonate platforms has been mainly controlled by the subsidence. However, the results highlight a strong overprint of eustatic fluctuations on the rates of change in accommodation, and hence on the stratigraphic architecture of the carbonate platforms. Based on an alternative model for the Cenozoic geodynamic evolution of the Yadana area, our results suggest that the platforms developed on a volcanic ridge of hotspot origin located in the Indian Ocean and not on a volcanic arc. Subduction jump processes are interpreted to have played a key role in the demise of all platforms by drastically changing the paleoenvironmental conditions during the Early Miocene, and led to the present-day location of the Yadana Ridge in a back-arc setting. The carbonate platforms from the Yadana area are thus a representative example of the interplay between global mechanisms and local paleoenvironmental parameters on carbonate platform initiation, growth and demise.

---

## Highlights

▶ Three carbonate platforms were developed in the Yadana area during the Late Oligocene - Early Miocene. ▶ These platforms show attached and isolated settings. ▶ Eustatic fluctuations affected their stratigraphic architecture. ▶ They were developed on a volcanic ridge of hotspot origin (Maldives type). ▶ Local environmental perturbations participated in the platform demise.

**Keywords** : Yadana, Carbonate platforms, Oligocene, Miocene, Seismic stratigraphy, Geomorphology, Paleogeography, Control parameters, Burman margin

## 1. Introduction

In SE Asia, the location, growth and demise of carbonate accumulations have been influenced by a combination of interacting mechanisms such as tectonics (including subsidence and paleotopography), eustasy, oceanography, climate, temperature, runoff, biota, siliciclastic supply, trophic resources and salinity (e.g. Kendall and Schlager, 1981; Fulthorpe and Schlanger, 1989; Greenlee and Lehmann, 1993; Wilson and Lokier, 2002; Hallock, 2005; Schlager, 2005; Lukasik and Simo, 2008; Wilson, 2000, 2008; Lokier et al., 2009). Conditions for the development of diverse and widespread shallow-water carbonates in this region were particularly conducive during the Cenozoic, thanks in part to the various passive and active tectonic settings creating a wide range of structural patterns (Fulthorpe and Schlanger, 1989; Wilson, 2002, 2008; Wilson and Hall, 2010).

Although ~70% of the SE Asian Cenozoic carbonate platforms initiated as attached features (Wilson and Hall, 2010), the majority of economic discoveries are located within isolated carbonate buildups (ICBs) (Greenlee and Lehmann, 1993; Wilson and Hall, 2010; Burgess et al., 2013). For example, ICBs form prolific hydrocarbon reservoirs in Indonesia (e.g. Rudolph and Lehmann, 1989; Jordan and Abdullah, 1992; Kusumastuti et al., 2002; Saller and Vijaya, 2002; Bachtel et al., 2004), in Malaysia (e.g. Epting, 1980, 1989; Vahrenkamp et al., 2004; Zampetti et al. 2004a, 2004b; Zampetti, 2010; Koša, 2015; Koša et

al., 2015), and in the Philippines (e.g. Grötsch and Mercadier, 1999; Neuhaus et al., 2004; Fournier et al., 2004, 2005). Consequently, the identification of ICBs (Burgess et al., 2013), the understanding of their regional development (Wilson, 2002, 2008; Wilson and Hall, 2010) as well as the accurate characterization of their reservoir properties and seismic expression (e.g. Fournier and Borgomano, 2007; Borgomano et al., 2008) remain a major challenge for the petroleum industry.

The Late Oligocene - Early Miocene Yadana Platform is located in the North Andaman Sea, offshore Myanmar, 80 km southward of the Irrawaddy River Delta (Fig. 1a), lying under 40 m of water. The Yadana Platform hosts a gas field operated by Total since 1998, which contains an Initial Gas in Place (IGIP) of around 7 trillion cubic feet. Other Oligocene - Miocene shallow-water carbonate platforms in the region have been found to be largely water-saturated. Understanding the paleogeography of these platforms and their evolution through time and space might help to identify coeval plays elsewhere in the region and improve the characterization of the Yadana Platform stratigraphic architecture and reservoir heterogeneities.

The structural evolution of SE Asia (including the Andaman Sea) during the Cenozoic is highly complex (Lee and Lawver, 1995, Hall, 1998, 2002, 2012). Available geodynamic models (e.g. Morley, 2013) suggest the presence of a volcanic arc where the carbonate production was initiated (intra-arc setting). However, the current conceptual models of the geodynamic evolution of the North Andaman Sea during the Cenozoic do not explain the creation of this volcanic arc. Moreover, the Yadana area is less extensively studied and seldom included in the numerous studies on the geodynamic evolution of the Andaman Sea (e.g. Curray et al., 1979; Kamesh Raju et al., 2004; Khan and Chakraborty, 2005; Curray, 2005; Radhakrishna et al., 2008; Chakraborty and Khan, 2009; Morley, 2002, 2012, 2013).

This study uses a combination of 2D/3D seismic surveys integrated with exploration well data in order to: (1) characterize the depositional environments and sequence stratigraphic architecture of the carbonate platforms; (2) reconstruct the paleogeographical evolution of these platforms from the Late Oligocene to Early Miocene; and (3) identify the main controls on the carbonate initiation, growth and demise (e.g. subsidence, eustasy).

## **2. Geological setting**

The complex tectonic evolution of SE Asia during the Cenozoic has strongly affected the distribution of lands and seas, leading to the current structural configuration of the region (Lee and Lawver, 1995, Hall, 1998, 2002, 2012). During the Paleogene, the northeastward oblique subduction of the Indian plate under the Eurasian plate (Fig. 1a) induced the opening of the Andaman Sea as a back-arc basin (Curry, 2005; Chakraborty and Khan, 2009). Because of the orientation of the subduction (northward motion of the Indian plate, almost parallel to the plate limit; Fig. 1a), a strong strike-slip component affects the Andaman Sea. This regional motion has created a WSW-ENE structural grain, leading to a complex system of spreading centers and transform faults (Curry et al., 1979; Curry, 2005; Fig. 1a). Relative to the Eurasian plate, the Burma microplate is distinguished by the creation of a major dextral strike-slip fault from the Eocene (the Sagaing Fault; Fig. 1a; Morley, 2002; Chakraborty and Khan, 2009).

According to this geodynamic scenario, the Yadana Platform would have been developed above a volcanic arc (Racey and Ridd, 2015), named the Yadana High (Figs. 1b and 1c) or the Yadana Arch (Morley, 2013). In this case, the M5 Basin (Figs. 1b and 1c) would correspond to a fore-arc basin and the Moattama Basin (Figs. 1b and 1c) to a back-arc

basin. The 3CA High (Figs. 1b and 1c) is located on the East part of the Yadana High and is founded on the volcanic arc complex, as well as the M8 High southward (Fig. 1b).

In the Yadana Platform, the stratigraphic succession is sub-divided as follows, from the oldest to the youngest (Fig. 2): (1) the volcanic basement; (2) the Lower Burman Limestone (LBL), Chattian in age; (3) the Sein Clastics Formation, which was deposited at the end of the Chattian; and (4) the Upper Burman Limestone (UBL), deposited during the Aquitanian. The main Yadana gas reservoir is located in the UBL (Fig. 2), with a gas column of 124 m and a gas extent of 65 km<sup>2</sup>. To the south, another gas accumulation exists in an uplifted area, bounded to the North by the Sein Fault (Fig. 2c). The LBL and UBL represent the main episodes of carbonate accumulation in the Yadana Platform with a cumulative thickness of ~500 m.

After a hiatus of ~15 My (Fig. 2), the Late Miocene (N17 planktonic foraminifera zone) pro-delta shales (forming the regional seal) of the Irrawaddy River Delta have prograded southward to progressively onlap the carbonate platforms and finally entirely bury them (Fig. 2). The M6 horizon (Fig. 1c), dated at 8.2 Ma (Late Miocene), reflects a major eastward tectonic tilt related to the Moattama Basin opening. During the Pliocene - Pleistocene, the Moattama Basin became a major depocentre (Fig. 1c), with the accumulation of over 10 km of terrigenous sediments, due to its transtensional opening and the supply of abundant sediments from the Irrawaddy River Delta (Fig. 1a). Southward, seafloor spreading initiated in the Central Andaman Basin ~4 Ma ago, at a rate of ~38 mm per year (Curray, 2005; Khan and Chakraborty, 2005; Chakraborty and Khan, 2009; Fig. 1a).

### **3. Data and methods**

#### *3.1. Well data*

The dataset is composed of twenty-one exploration wells, including YAD-1, and three appraisal wells YAD-2, 3 and 4 (Fig. 1b). Information from relevant wells crossing the carbonate strata, coming from well completion reports and proprietary geological reports, include: age from micropaleontology; cuttings description; wireline logs interpretation (gamma ray, sonic, porosity, density and resistivity); sedimentological description of ~600 m of cores; and sedimentological description of ~345 sidewall cores (e.g. in the well M6A-1 with a 2 m sampling in some parts). Refined studies were also carried out by TOTAL on the Yadana reservoir (high-resolution semi-quantitative and qualitative studies), where the entire UBL top is cored on a ~100 to 150 m interval. This paper includes the interpretations derived from these previous proprietary reports to provide basic information on the relationship between seismic observations and depositional environments.

### *3.2. Seismic data*

The seismic data used in this study includes 2D and 3D seismic data (Fig. 1b). The 2D seismic data was acquired between 1993 and 1997 covering an area of ~14 200 km<sup>2</sup>. From this 2D data, the base of the regional seal was interpreted (Fig. 1b). The 3D seismic data, acquired in 2011, mainly covers the Yadana, Badamyar and Sein gas fields in an area of ~511 km<sup>2</sup>. The 3D volume is characterized by a bin spacing of 12.5 x 6.25 m. The data are of very good quality, except below gas chimneys (e.g. Sein gas field area). The seismic sampling is 3 ms and the vertical resolution is 18 m for a central frequency of 45 Hz.

Carbonate buildups were interpreted on seismic data using the identification criteria of Burgess et al. (2013). Seismic stratigraphic analysis was conducted on Sismage<sup>®</sup> (TOTAL in-house) software which allowed identification of the main seismic unconformities and their

associated seismic sequences (*sensu* Mitchum et al., 1977a). Within each identified seismic sequence, the platform margins were mapped and the seismic facies were identified throughout. Seismic facies were mapped on 2D seismic data at the top of each Late Oligocene - Early Miocene seismic sequence, corresponding to a window of ~50 ms TWT along each seismic unconformity. The seismic facies were interpolated regionally and displayed on paleogeographical maps ranging from the Chattian to the Burdigalian.

Seismic attributes were extracted from the 3D seismic data just below key seismic unconformities over a time window of  $\pm 20$  ms TWT in order to investigate the geomorphology (e.g. Posamentier et al., 2010; Menier et al., 2014) of the Yadana Platform and its evolution through time and space. Major discontinuities (e.g. faults, platform margins, karst features) were highlighted by using the *coherency* attribute, which compares the similarity of a trace with the others in all the directions on an interpreted surface (Masferro et al., 2004; Chopra and Marfurt, 2007). The *Root Mean Square (RMS)* attribute, which is an amplitude extraction over a given interval (Masferro et al., 2004; Chopra and Marfurt, 2007) has been used to discriminate different carbonate depositional environments (e.g. reef rims, lagoons, patch reefs). Finally, the *spectral decomposition* attribute, which consists of the creation of a blended RGB (red-green-blue) composite map of different frequency maps calculated in an analysis window (Chopra and Marfurt, 2007), helped to characterize heterogeneities and sub-seismic scale geological features (e.g. changes in thickness and depositional facies).

## 4. Results

### 4.1. Seismic facies analysis on 2D seismic data

Examination of the 2D seismic data allowed the description of six main seismic facies (Fig. 3). Each seismic facies is defined from its reflection properties (amplitude, internal geometries, continuity and terminations) at the scale of ~50-200 ms TWT vertically and ~1-3 km laterally (Fig. 3).

#### *4.1.1. Seismic facies 1 (SF1) and 2 (SF2): parallel seismic reflectors*

SF1 and SF2 consist of sub-horizontal to horizontal parallel and continuous reflectors of high amplitude (Fig. 3). They form relatively thick packages of ~100 to 250 ms TWT (Fig. 3). SF1 is identified basinward of the toe of slope of the carbonate platforms, where it can be continuous for tens of kilometres. The seismic reflectors are mostly parallel to the seismic unconformities and in some cases can directly onlap the carbonate platform margins. SF2 is identified in a platform interior position with reflectors parallel to the overlying and underlying seismic unconformities without presenting any particular reflection termination pattern. Laterally, SF2 is transitional with the SF5 and / or the SF6 seismic facies and displays in some locations a slight wavy internal configuration (Fig. 3). For both seismic facies SF1 and SF2, the reflectors present in some cases a concave-down configuration.

#### *4.1.2. Seismic facies 3 (SF3) and 4 (SF4): high-angle clinoforms*

SF3 corresponds to oblique parallel to slightly tangential clinoforms of moderate to high amplitude dipping basinward (Fig. 3). They form high-angle (~3 to 6°) and ~100-300 ms TWT high semi-continuous to continuous reflectors (Fig. 3) located at the level of the platform margin which can pass basinward to the seismic facies SF1. These clinoforms are arranged in packages of 1-3 km long in dip view and their lower reflection terminations are

characterized by downlaps (Fig. 3). Seismic facies 4 (SF4) is characterized by sigmoidal clinoforms with preserved toplap and downlap terminations (Fig. 3). Similarly to SF3, the semi-continuous to continuous reflectors present a moderate to high amplitude (Fig. 3). They form high-angle (up to  $\sim 8^\circ$ ),  $\sim 3$ -6 km long and  $\sim 50$ -150 ms TWT high clinoforms (Fig. 3) which are transitional with the seismic facies SF1 basinward or the seismic facies SF2 towards the platform interior.

#### *4.1.3. Seismic facies 5 (SF5): mounded seismic reflectors*

SF5 is characterized by low to moderate amplitude convex-up (mound shape) discontinuous to semi-continuous reflections with bidirectional downlaps, forming  $\sim 20$ -30 ms TWT thick packages (Fig. 3). When located close to the platform margins, SF5 is  $\sim 0.5$  to 2 km wide (Fig. 3) and can be extended long distance (up to 20 km). In this case, SF5 is often transitional with SF6 toward the platform interior and can pass abruptly to the seismic facies SF3 or SF1 basinward. When located within the platform interior, this seismic facies can be smaller ( $< 0.5$  km wide) and thinner ( $< 20$  ms TWT).

#### *4.1.4. Seismic facies 6 (SF6): chaotic seismic reflectors*

SF6 presents highly disrupted, chaotic to wavy, discontinuous reflections of low amplitude organized in  $\sim 10$ -150 ms TWT thick packages (Fig. 3). This seismic facies is located between the seismic facies SF5 and SF2 within the carbonate platforms, and rarely, directly at the platform margin.

### *4.2. Seismic stratigraphy*

The carbonate platforms were identified following geometrical and geophysical observations (Bubb and Hatlelid, 1977; Burgess et al., 2013; Figs. 4-9): e.g., positive antecedent topography, significant thickening, high-angle slope, onlap of overburden sediments, stacking patterns (progradational, aggradational and retrogradational) and presence of karst features. These criteria have allowed the identification of three main carbonate platforms (Fig. 7a): Yadana, 3DF and 3DE.

Following a standard seismic stratigraphic approach (Mitchum et al., 1977a, 1977b; Vail and Mitchum, 1977), several key stratigraphic surfaces (seismic unconformities) and seismic sequences have been identified (Figs. 4-9). Above U0 (top of volcanic basement), seven seismic unconformities (U1 to U7) were identified (Figs. 4-9), encompassing seven seismic sequences (S1 to S7) which can be followed regionally. Each seismic unconformity has been reported in depth on the well sections (Figs. 4d and 5d).

#### *4.2.1. Seismic sequence S1: Late Eocene*

Above the volcanic basement, S1 has been observed only in the western part of the study area, at the base of the 3DF Platform (Figs. 4 and 8). The biostratigraphic data in the well 3DF-X points to a Late Eocene age for S1 (NP18-20). This sequence is bounded at its top by the seismic unconformity U1 which corresponds to a downlap surface of the overlying sequence (Fig. 8). This thin sequence (~10 to 75 ms TWT) consists of sub-parallel continuous reflectors of high amplitude thinning toward the east (Fig. 8).

#### *4.2.2. Seismic sequence S2: Chattian (LBL)*

S2 is well developed on each platform (Figs. 4-9) and corresponds to the LBL (Fig. 2), although a thin clastic layer at the base of the Yadana Platform can be observed in some wells (e.g. 3DA-XA; Fig. 4). Age control on the Yadana Platform is derived from biostratigraphic data, which yields a Chattian age (NP24-25; Fig. 2). Precise biostratigraphic data is unavailable or of very poor quality (out of date) on the other platforms, and so their geologic age is inferred from regional seismic correlations. S2 is bounded at its top by the seismic unconformity U2 which corresponds laterally to an onlap surface (Figs. 4-9) and vertically to a downlap surface of the overlying reflectors (e.g. in the Yadana Platform; Fig. 6). Some ~10 ms TWT deep erosional truncations are evident along this unconformity (e.g. in the 3DF Platform; Fig. 8). S2 presents variable thicknesses (~300 ms TWT in the 3DF Platform and ~150 ms TWT in the Yadana Platform; Fig. 4). Moreover, in the Yadana Platform, S2 includes a pronounced thinning (~50 ms TWT; Fig. 6) over a width of 3 km, highlighting a NE-SW trough which can be followed for 30 km. Local internal progradations are evident in the eastern part of the 3DF Platform (Fig. 8).

#### 4.2.3. Seismic sequence S3: Late Chattian (Sein Clastics Formation)

Developed in the trough described in the Yadana area (Fig. 6) and bounded at its top by the seismic unconformity U3, sequence S3 (Figs. 4 and 5) displays ~2 to 3 km long and ~100 ms TWT high (~150 m) prograding high angle (~5°) sigmoidal clinoforms downlapping the seismic unconformity U2 (Fig. 6). This interval corresponds to the Sein Clastics Formation (Fig. 2) as highlighted by a number of wells in this trough (e.g. 3DA-XA, 3DA-XC; Fig. 4), with biostratigraphic data suggesting a Late Chattian age (NP25; Fig. 2). Sequence S3 appears to be largely confined to the Yadana trough, with only limited development outside this depression (Fig. 6). Two wells (e.g. 3DA-XB, YAD-1; Fig. 5)

penetrate the Sein clastics formation outside the trough to the south of the Yadana platform (Fig. 6). These wells allow the interpretation of the top bounding seismic unconformity U3 toward the south where S3 is reduced to a thickness of ~30 ms TWT (Figs. 6). However, the interpretation of this horizon remains difficult due to a combination of faulting and poor seismic resolution in this area. Toward the north, U3 onlaps the seismic unconformity U2 and forms a small trough (Fig. 6). No evidence of this clastic sequence has been found in the 3DF-X and 3DE-1 platforms (Figs. 4).

#### 4.2.4. Seismic sequences S4 to S6: Aquitanian (UBL)

Above U3, three additional seismic unconformities (U4 to U6) have been defined on both the 3DF and Yadana platforms, bounding respectively the seismic sequences 4 to 6 (S4 to S6; Figs. 4 and 5). Those seismic sequences correspond to the Aquitanian in age (NN1-2; Fig. 2) Upper Burman Limestone (UBL; Fig. 2). However, no precise biostratigraphic data is available to date each individual unconformity which are thus defined only on the seismic stratigraphic interpretation and correlation. As for U2, these seismic unconformities are defined by onlaps laterally off the margins of the platforms (Figs. 4-9). Vertically, the seismic unconformity U4 has been defined as a downlap surface of overlying high-angle clinofolds (i.e. seismic facies SF4) in the eastern part of the Yadana Platform (Fig. 4). On the 3DF Platform, U4 downlaps directly on the U2 surface toward the East (Fig. 8). This first Early Miocene sequence (S4) has a similar thickness on all platforms (~75 to 100 ms TWT). Additionally, S4 constitutes the last seismic sequence developed on the 3DE Platform (line C-C'; Fig. 9). Here the U4 surface is onlapped and overlain by Middle Miocene sediments (NN6-7) highlighting a hiatus of ~8 My. On the Yadana and 3DF platforms, the seismic unconformity U4 is overlain by the seismic sequence S5 whose top bounding seismic

unconformity (U5) downlaps horizon U4 in the east part of the Yadana Platform (Fig. 4) and horizon U2 in the 3DF Platform (Fig. 8). The seismic sequence S5 itself shows internal geometries downlapping the underlying sequence (e.g. in the 3DF Platform; Fig. 8). In the Yadana Platform, S5 includes a ~20 to 30 km backstepping event from the entire initial extent (Figs. 4 - 6). Thus, S5 displays a thickness of about 100 ms TWT in the western and southern parts (e.g. from the Nilar Fault to the platform margin; Fig. 5) except in the uplifted area (~50 ms TWT) where erosion has perhaps removed a part of the carbonate succession (e.g. between the Nilar Fault and the Sein Fault; Fig. 5). Seismic sequence S5 reaches a maximum thickness of ~200 ms TWT on the 3DF Platform (Figs. 4 and 8) and ~150 ms TWT on the north part of the Yadana Platform (Figs. 4-6). On the Yadana Platform, S5 displays an internal downlap surface (Fig. 6) that could be defined as a seismic unconformity. However, S5 was not subdivided internally due to the lack of regional seismic correlation with the other carbonate platforms (Figs. 4 and 5). Other similar surfaces were identified in S5 and are interpreted to represent different stages of backstepping. The final seismic unconformity (U6) is the last backstepping feature on the two platforms (Figs. 4-8) and downlaps the underlying seismic unconformity U5. This last sequence shows a greater thickness on the 3DF Platform (~60 ms TWT) than on the Yadana Platform (~40 ms TWT). Toward the south part of the Yadana Platform, the seismic sequences S2 to S4 onlap the 3CA High (Fig. 7). Basinward, the seismic unconformities U2 and U4 are interpreted throughout the North Depocenter (Fig. 5) as correlative seismic conformities, and tied to well 3CA-A2, where carbonates of Chattian to Aquitanian age were identified in this interval (Fig. 5). However, to the east, the 3CA High constitutes a highly faulted area where low seismic resolution combined with the presence of volcanic rocks (Figs. 4 and 5) makes the interpretation of seismic unconformities and their correlation with the carbonate platforms to the west difficult.

#### 4.2.5. Seismic sequence S7: Burdigalian

The regional unconformity U7 has been interpreted at the top of the various volcanics in the 3CA area (Figs. 4 and 5). This surface onlaps the Yadana Platform toward the west (Figs. 4 and 5) and corresponds to the top of the seismic sequence S7 (line D-D'; Fig. 9). This sequence corresponds to a package of high amplitude reflectors with parallel geometries in the North Depocenter (Fig. 5) and displays a chaotic configuration on the 3CA High (Figs. 4 and 5). From well data (e.g. 3CA-2; Fig. 5), this sequence corresponds to volcanic deposits (e.g. tuffs, agglomerates, ashes) which is consistent with the identification of lava flows on seismic (line D-D'; Fig. 9). In the wells 3CA-2 and M6A-1 (Fig. 5), shallow-water carbonates were identified above the volcanic deposits. Biostratigraphic data indicates a Burdigalian age (NN2-3) for these carbonates. In the well M6A-1 (Fig. 5), the carbonates are interbedded with shales and sands including volcanic materials (e.g. tuff) suggesting a mixed deposition of clastic, volcanic and carbonate sediment.

#### 4.3. Yadana 3D seismic geomorphology

Attribute analysis of the Yadana Platform (3D seismic data) was conducted along the interpreted seismic unconformities U2 (Fig. 10) and U6 (Fig. 12). Discontinuities observed on the coherency attribute map correspond to faults and platforms margins. Identification of the latter helps to spatially define the different geomorphological features. Based on the coherency (e.g. Fig. 10a), the amplitude (e.g. Fig. 10b), the spectral decomposition (e.g. Fig. 10c) and the shape (plan view geometry), seven main architectural elements (AE; *sensu* Pickering et al., 1989) were identified (Table 1). Each AE was compared to the seismic facies previously described (*see section 4.1.*).

Along seismic unconformity U2 (Fig. 10), the margins of two platforms were identified, suggesting that during S2, two distinct carbonate platforms developed, the Yadana North Platform (YNP; Fig. 10) and the Yadana South Platform (YSP; Fig. 10), which were separated by an elongated trough defining a SW-NE interplatform seaway.

Off the platform margins, AE1 and AE2 (Table 1) are characterized by low frequencies (Fig. 10). AE1 is located in the most distal parts and is associated with strong amplitudes; whereas AE2 surrounds the platform margins and displays moderate amplitudes (Fig. 10). In terms of seismic facies, AE1 is associated with parallel seismic reflectors (i.e. SF1; Fig. 3) and AE2 with parallel oblique clinoforms (i.e. SF3; Fig. 3). Within the latter, concentric discontinuities (separated by a distance of ~0.5 to 1 km) are observed on the coherency map (e.g. YNP; Fig. 10).

Within the platform interior, AE3 (Table 1) is defined by low amplitudes and frequencies located along the platform margins (Fig. 10). In some areas, AE3 is spatially extended ~2-3 km toward the platform interior (e.g. YNP; Fig. 10); whereas other occurrences are smaller (~1 km across) and display narrow discontinuities <500 m (Fig. 10). AE3 is commonly associated with a mounded seismic facies (i.e. SF5; Fig. 3) and in some cases with a chaotic seismic facies (i.e. SF6; Fig. 3). Distributed randomly within the carbonate platforms, the AE6 (Table 1) presents the same seismic characteristics as AE3 in terms of amplitudes and frequencies, with the exception that this AE displays a sub-circular shape highlighted by a discontinuity on the coherency attribute map (Fig. 10). AE6 displays a wide range of sizes, from ~50 to 500 m, and is linked with a mounded seismic facies (i.e. SF5; Fig. 3).

The architectural element AE4 (Table 1) is associated with a chaotic seismic facies (i.e. SF6), and displays low to moderate amplitudes and frequencies (Fig. 10). As within AE3, two distinct spatial configurations are observed in AE4. In the first case (e.g. YNP; Fig. 10),

AE4 is very wide (~5 to 8 km), parallel to the platform margin, and located between the architectural elements AE3 and AE5 (described hereafter). In the second case (e.g. YS; Fig. 10), AE4 is less evenly distributed, with a sparse distribution toward the platform interior making its identification challenging. In some cases, distinguishing between of AE4 and AE6 is made difficult by their similar seismic character (e.g. Fig. 10). Differences however, can be seen in their shape (Fig. 10) and seismic facies (Fig. 3).

Architectural element AE5 is located in the most internal position (in regards to the platform margin) (Table 1), and shows both high amplitude and frequencies on attribute maps (Fig. 10). This AE is linked with the seismic facies SF2 which corresponds to parallel seismic reflectors (Fig. 3 and Table 1).

The last architectural element AE7 (Table 1) corresponds to sub-circular features highlighted by sub-circular discontinuities on the coherency map located within the platform interior (Fig. 10). They present high amplitudes and moderate to high frequencies. AE7 is associated with a chaotic seismic facies (SF6; Fig. 3) and in some cases, with erosional features ~10 ms TWT deep. Most of these features are ~100 to 500 m wide, with the largest reaching ~1 km in width.

## **5. Interpretation**

### *5.1. Seismic facies and geomorphological features*

An interpretation of the previously identified seismic facies (Fig. 3) and architectural elements (Fig. 10 and Table 1) is proposed in Figure 13. To help the interpretation of the observed geometries, the architectural elements were compared to modern analogues (e.g. Fig. 11). The interpretation of seismic facies is helped by a scheme developed in a similar

carbonate setting by Bachtel et al., 2004 (Fig. 3). The paleogeography of the Yadana area can be subdivided into five main depositional environments or geomorphological areas (Fig. 13), namely: deep volcanic shelf, slope, reef barrier, back-reef (apron, sandwaves, shoal) and lagoon or inner-platform.

SF1 and AE1 (Figs. 3 and 10; Table 1) are interpreted as a deep volcanic shelf depositional environment (*sensu* Schlager, 2005; Fig. 13). Well data located around the toe of slope of the platforms highlights the presence of carbonate mudstone associated with thin layers of marls and claystone, suggesting hemipelagic sedimentation. These peri-platform carbonates are rich in planktonic foraminifera. The identification of thin-bedded platform-derived materials containing shallow-water benthos (e.g. coralline algae) is interpreted as the result of distal gravity processes (e.g. turbidites; Fig. 13) occurring along the toe of slope of the platforms. We use the term deep volcanic shelf to name all the peri-platform areas on top of the volcanic basement (i.e. Yadana High; whereas the adjacent basins (i.e. M5, Preparis and Moattama; Fig. 1b) correspond to oceanic deep-water (>1000 m water depth).

Located basinward of the platform margins, SF3 and SF4 are interpreted as a platform slope depositional environment (Figs. 3 and 13). In the Yadana area, well control is poor but available data shows grain-supported facies dominated by foraminifera (e.g. *Cycloclipeus sp.*) interbedded with rudstone containing red algae and coral debris. The slope is thus interpreted to be mainly composed of reworked sediments derived from the platform (Schlager, 2005; Fig. 13), which is consistent with the seismic facies displaying relatively high inclination (3 to 8°; Fig. 3). We infer that the discontinuities observed in the AE2 (Fig. 10 and Table 1) correspond to ancient platform margins or reef flats developed during platform growth as seen on slopes of modern carbonate platforms (e.g. Jorry et al., 2016).

The seismic facies SF5 is identified either at the platform margin or within the platform interior (Fig. 3). We interpret this seismic facies to be representative of a reef

depositional environment characterized by a vertical growth giving the mound shape to the seismic facies (e.g. Bachtel et al. 2004) (Figs. 3 and 13). When developed at the platform margin, SF5 is interpreted as a barrier reef rimming the carbonate platform (Figs. 3 and 13). This is consistent with the identification of the AE3 presenting either crescent (e.g. YNP; Fig. 11) or elongate (e.g. YNS; Fig. 11) geometries along the platform margin as observed on modern examples (Figs. 11 and 12). Here we propose that the barrier reef includes both the reef crest and the reef flat. When developed within the platform interior, correlation of SF5 with AE6 (Figs. 3 and 10; Table 1) allows interpretation of platform interior reefs (patch reefs) (Fig. 13). Laterally toward the platform interior the barrier reef depositional environment is often associated with the seismic facies SF6 (Fig. 3), as illustrated on the 3DF Platform (Fig. 8). SF6 is thus interpreted as a back-reef or apron depositional environment (Figs. 3 and 13). Such environments can be composed of debris shed from the barrier reef (when present) or sandwaves, giving the chaotic configuration to the seismic data (Fig. 13). In some cases, SF6 is located directly at the shelf margin and can be defined as a shoal depositional environment (*sensu* Schlager, 2005; Fig. 13). On the attribute maps, the corresponding architectural element is AE4 (Fig. 10 and Table 1). AE4 presents either a geometry parallel to the reef barrier (e.g. Fig. 12) (consistent with a back-reef depositional environment as exemplified on a modern atoll from the Maldives (Fig. 12)); or a sparse configuration which makes its interpretation difficult (e.g. YSP; Fig. 11). Similar complexity can be observed in modern settings (Fig. 11e) with various geomorphological features observed, including apron deposits and sandwaves (Jorry et al., 2016; Prat et al., 2016). However, these fease features often lie below seismic resolution and thus a general back-reef (apron) depositional environment is assigned here (Fig. 13). These two marginal depositional environments (barrier reef and back-reef) contains a wide range of sedimentary facies which constitute the Yadana reservoir (Fig. 2). These high-energy facies observed in the cores from

the top of the Yadana Platform (not detailed here) are mostly grain-supported (packstone, grainstone, boundstone, rudstone) and include variable amounts of shallow-water biota, dominated by coralline algae, large benthic foraminifera and corals. The back-reef depositional environment is in most cases characterized by either coral / red algae debris (interpreted as the apron); or by foraminifera dominated (e.g. *Lepidocyclina sp.*) grainstone.

SF2 and AE5 (Figs. 3 and 10; Table 1) are located in a platform interior setting which can be defined as an inner-platform or lagoon depositional environment (Fig. 13). In some areas, SF2 displays slightly concave reflectors (e.g. Yadana Platform; Fig. 4) suggesting a differential compaction when compared to the platform margin where SF5 (i.e. barrier reef) is identified. This infers the presence of fine-grained sediments indicative of a low-energy environment. If a reef barrier does not rim the entire platform, SF2 and AE5 are interpreted as an inner-platform (or open lagoon) depositional environment (*sensu* Schlager, 2005), as exemplified by the contemporary Glorieuses Archipelago (Prat et al., 2016; Jorry et al., 2016). If a barrier reef encloses the entire platform, a lagoonal depositional environment can be attributed (*sensu* Schlager, 2005; Fig. 13).

AE7 (Fig. 10 and Table 1) is interpreted as a sinkhole feature (Fig. 13), potentially developed during a period of subaerial exposure. Such a feature is developed on the YSP (Fig. 11) and is well observed with the spectral decomposition attribute (Fig. 11c). In this case, AE7 is almost entirely surrounded by the AE6 (interpreted as a reef), forming a striking similarity with the geometry of the “Blue Hole” observed in the Belize Barrier Reef (Fig. 11d). This configuration suggests that after the emersion, the flooding of the platform allowed the development of these reefs around the sinkhole boundary. A similar sinkhole is observed at the top of the Yadana Platform (Fig. 12) suggesting a final phase of emersion of the platform. In this case, the sinkhole is deep (~25 ms TWT; Fig. 12e) and seems to present two distinct areas (Fig. 12d). By comparing with a sinkhole developed during the Last Glacial

Maximum (LGM) on the reef flat of the Glorieuses Archipelago (Fig. 12f), we interpret these two areas as shallow and deep depressions, respectively. The relief has probably been enhanced by the surrounding reef growth (Jorry et al., 2016; Fig. 12e).

## *5.2. Paleogeographical evolution*

Six paleogeographical maps were created, ranging from the Chattian to the Burdigalian (Fig. 14). The paleogeographical evolution is detailed hereafter for each carbonate platform.

### *5.2.1. The Yadana Platform*

The Yadana Platform is a wide platform with a maximum extent of approximately 75 by 35 km at the beginning of the Aquitanian (Fig. 14). However, during the Chattian (Fig. 14), two carbonate platforms developed (YNP and YSP), separated by a narrow (~3 km wide) interplatform seaway (Figs. 10, 11 and 14). Seismic data suggests that the seaway could be fault-controlled with SW-NE normal faults identified at the base of the seaway (Fig. 5) and / or affected by strong currents giving its linear morphology. Similar seaways or channels are observed today in the Maldives (Fig. 11b). The isolated YNP platform presents a prominent crescent barrier reef and west-trending apron (Fig. 11). The YNP platform reaches ~30 km in the SW-NE direction, interpreted as the windward side of the platform, and features a small (~8 km wide) lagoon (Fig. 11). Toward the opposite margin of the platform, identification of SF2, and the lack of barrier reef (Fig. 13), is indicative of a shoal depositional environment (Fig. 14). This is consistent with the interpretation of the AE4 on the eastern limit of the 3D survey (Figs. 10 and 11). On the western side, interpreted in as the windward margin, the

identified ancient platform margins (Fig. 10) are indicative of backstepping events (a retrogradational pattern) during platform evolution. The YSP is much larger than the YNP, reaching ~55 km in the SW-NE direction (Fig. 14). A barrier reef is observed along the margin associated with an apron / lagoon complex (Fig. 11). The barrier can be followed southward until reaching the M8 High (Fig. 14). Some toe of slope debris are identified downdip of this barrier reef and interpreted as the downslope shedding of platform debris (Fig. 5). Numerous patch reefs are visible across the entire platform (Figs. 11 and 14). Despite the poor quality of the seismic toward the south and the presence of closely spaced faults (Pliocene - Pleistocene age), seismic interpretation suggests that the YSP corresponds to a rimmed platform attached to the 3CA High (Figs. 7 and 14), as evidenced by: (1) onlap and thinning of the seismic sequence S2 on the 3CA High all along the margin ; (2) identification of the seismic facies SF2 interpreted as a lagoon (Fig. 3); and (3) presence of the isolated mounded seismic facies (SF5) interpreted as patch reefs (Fig. 3). The 3CA High is thus interpreted as a paleohigh exposed during the Chattian which supplied terrigenous clastic sediments to the system (Fig. 14). Silt and clay are interbedded with the shallow-water carbonates of the seismic sequence S2 approximately ~30 km from the volcanic source (e.g. well M5A-1; Fig. 5) which could be interpreted as distal sedimentary plumes (Fig. 14).

Seismic evidence of sinkholes at the top of S2 suggests an emersion of the Yadana Platform at the end of the Chattian (Figs. 11 and 14). Due to the attached setting of the YSP, we infer that siliciclastic bypass occurred across this subaerially exposed shelf, allowing the development of S3 in the trough between YSP and YNP (Fig. 14). Sediments (sourced from the 3CA High) were delivered to the north platform margin and accumulated within the SW-NE interplatform seaway where accommodation space was available (Fig. 14). This interpretation is consistent with the north dipping clinofolds identified in the seaway (Fig. 6) indicating transport from the SE to the NW. This contrasts with previous interpretations

suggesting a source from the paleo Irrawaddy River Delta in the north (Mitra, 2005). The sandstone described in the wells (e.g. 3DA-XC; Fig. 4) contains siliciclastics, mafic minerals (e.g. pyroxene, olivine) and volcanic fragments, suggesting a volcanogenic origin of the material (3CA High; Fig. 14). This volcanoclastic layer is not found on the YNP, probably due to the confinement of the sediments into the seaway (Fig. 14). Excess sediments may have been transported along strike toward the M5 Basin (Fig. 14) by channelized currents (Fig. 7). To explain the transport of sediments from the 3CA High to the trough, we infer the presence of fluvial systems as the main transport mechanism for clastic sediments (Fig. 14). Fluvial transport may be evidenced by the poor grain maturity of the sands (i.e. poorly sorted, angular to sub-rounded) described in the wells located in the seaway (e.g. 3DA-XC; Fig. 4) and on the shelf (e.g. 3DB-A; Fig. 5). Analogous development of fluvial systems on attached carbonate platforms has been documented during the LGM: e.g., the Belize Barrier Reef (Droxler and Jorry, 2013); and Nouméa lagoon (Le Roy et al., 2008). However, neither fluvial geomorphologies nor incised valleys appear on the seismic data (cross-sections or attribute maps) which suggests that either these features are sub-seismic, or that rivers did not incise the shelf during emersion, in similarity to the Great Barrier Reef (Woolfe et al., 1998). Within S3 on the YSP, small-scale (~200 m across), low amplitude features, interpreted as the seismic facies SF5 are observed (Fig. 6f). These are interpreted as small patch reefs onlapped by the clastic layer.

After this uppermost Oligocene clastic sequence, and the filling of the entire interplatform seaway, one single large Yadana Platform is developed at the beginning of the Aquitanian (Fig. 14). The platform is bounded by one large barrier reef on its western side which thins toward the north and the east (Fig. 14). Apron deposits are linked to this barrier (Fig. 14). In the south, the platform is still attached to the 3CA High which continued to provide clastic sediment into the lagoon (Figs. 14). A stepwise backstepping of the Yadana

Platform initiated during S5 (Aquitanian in age) which ultimately reduced the Yadana Platform to a sub-circular platform of ~25 km diameter (Fig. 14). A last backstep occurred during S6 as the platform reached its minimum extent of ~20 km (Fig. 14). The paleogeography is similar for the two seismic sequences S5 and S6 (Fig. 14): a large crescent barrier reef in the west, interpreted as the windward side, associated with apron deposits and a lagoon. However, seismic data does not show any barrier reef on the opposite margin, leading to the interpretation of an open platform with an inner-platform depositional environment (Fig. 14). This open-marine setting may have facilitated the export of sediments from the inner-platform basinward, highlighted by the presence of the seismic facies SF4 in the east (Fig. 4).

#### 5.2.2. The 3DF Platform

The Late Eocene base of the 3DF Platform (seismic sequence S1) corresponds mainly to a packstone / grainstone lithology dominated by large benthic foraminifera associated with red algae (3DF-X well; Figs. 4 and 8). High amplitude parallel reflectors (SF2; Fig 3) are observed and associated with a thinning toward the East (Figs. 4 and 8), which could be interpreted as a carbonate ramp.

During the Chattian (seismic sequence S2; Fig. 14), the 3DF Platform (Fig. 8) is a large isolated carbonate platform (~25 to 30 km in diameter). 3DF forms a sub-circular platform with two symmetrical reef margins, consistent with an atoll configuration (*sensu* Tucker and Wright, 1990) (Fig. 14). On the west side of the platform, an internal onlap surface shows the position of the platform margin (Fig. 8). Thus, the adjacent deposits toward the west correspond to periplatform carbonates (Figs. 8 and 14). Along the slope on the east side of the platform, three terraces are present and interpreted as ancient reef flats

corresponding to ancient platform margins (Fig. 8). A ~1 km wide barrier reef surrounds the entire platform, associated with large concentric apron deposits (Fig. 14). Internally, the platform presents a lagoon associated with numerous patch reefs (Figs. 8 and 14). Visible local internal progradations adjacent to a normal fault in the 3DF Platform suggests that faulting was still active during S2 deposition (Fig. 8).

Similarly to the YSP and YNP, the erosional truncation observed along the seismic unconformity U2 suggests that the 3DF Platform was subaerially exposed during the Oligocene - Miocene transition (Figs. 8 and 14). However, the seismic sequence S3 is not observed and the successive Aquitanian sequences (S4 to S6) instead lie directly on top of the U2 unconformity (Fig. 8). During the development of the seismic sequences S4 and S5, the 3DF Platform displays an asymmetric configuration. While the eastern side of the platform shows a retrogradational pattern, the western side still represents an aggradational margin (Fig. 8). During this interval, a prominent barrier reef is developed on the western side of the platform (interpreted as the windward side) associated with a large apron (Fig. 14). In S4, long oblique parallel clinoforms (Fig. 8) result from the progradation of carbonate sediments toward the platform interior. On the eastern side of the platform, a smaller barrier reef is present at the end of S4 and encloses a wide lagoon with patch reefs (Fig. 14). After backstepping, the 3DF Platform returns to a more symmetric shape (i.e. atoll-like) during S6 with a concentric barrier reef and apron interpreted all around the platform enclosing a lagoon (Fig. 14).

### 5.2.3. *The 3DE Platform*

The 3DE Platform is a small-scale platform elongated in the NE-SW direction (7 km length and 2 km width), separated from the 3DF Platform and the Yadana Platform by two

SW-NE oriented seaways (Fig. 14). The 3DE Platform seems to have been initiated on top of a small paleotopographic high with three coalescing aggrading buildups (line C-C'; Fig. 9). The well 3DE-1 (line C-C'; Fig. 9) crosses one of these buildups (SW side) and available core data shows a grainstone to boundstone lithology dominated mainly by corals, coralline algae and large benthic foraminifera, and interpreted as a reef facies. Thus, each one of the buildups can be defined as reefal bioherms forming a wider complex corresponding to the 3DE Platform (Fig. 14). This platform presents the same paleogeographical configuration during the Chattian (S2; Fig. 14) and the Aquitanian (S4; Fig. 14) before its final demise.

#### 5.2.4. *The 3CA High*

During the overall carbonate depositional history (S1 to S6; Fig. 14), the 3CA High is interpreted as a permanent paleohigh (volcanic origin), constituting a source of clastic sediments. However, renewed volcanic activity (likely initiating in the Aquitanian), occurred as indicated by the presence of large volcanoes and associated lava flows (line D-D'; Fig. 9), forming the seismic sequence S7 (Figs. 4 and 5). This sequence also contains Burdigalian shallow-water carbonates developed concomitantly or just following volcanic activity (Figs. 4 and 5). The seismic data does not allow determination of specific platform features, except some bioconstructions (e.g. Figs. 4 and 5); whereas shallow-water carbonate facies are clearly identified in the wells (e.g. 3CA-2, M6A-1; Fig. 5). The paleogeography proposed in Figure 14 therefore remains highly interpretative, however it is supported by data from the well M6A-1 (Fig. 5). In this area, we infer the presence of fringing reefs developed around the remnant eroded paleorelief (3CA High) and / or around the newly formed volcanoes (Fig. 14). Clastic sediments (volcanogenic material) were also supplied to the system from the adjacent relief as highlighted in the well M6A-1 (Fig. 5). The bioconstructions observed (e.g. Fig. 4)

can be interpreted as small-scale isolated carbonate buildups developed on the flooded volcanic shelf (Fig. 14).

## 6. Discussion

### 6.1. Controls on carbonate growth and architecture: subsidence and eustasy

Sea-level plays a key role in the stratigraphic evolution of carbonate platforms (Kendall and Schlager, 1981; Handford and Loucks, 1993), as the available accommodation space directly impacts the carbonate producers on biotically controlled tropical carbonate platforms (Tucker and Wright, 1990; Schlager, 2005). In this study, the development of the different seismic sequences (S1 to S7) can be linked to relative sea-level variations (i.e. rates of change in accommodation), which in turn are the results of the interplay between eustasy, subsidence and carbonate production (Kendall and Schlager, 1981; Schlager, 2005; Lukasik and Simo, 2008).

The carbonate platforms of the Yadana area document two major periods of carbonate aggradation; during the Chattian (S2; Fig. 15a) and the Aquitanian (S4 to S6; Fig. 15c). These phases, defined as transgressive megasequences, can be interpreted as the result of long term sea-level rise (Kendall and Schlager, 1981). Both megasequences present aggrading and backstepping features (Figs. 15a and 15c). However, while the Chattian megasequence is mainly aggrading with minor backstepping, the Aquitanian megasequence is characterized by km-scale backstepping stages (Figs. 15a and 15c) on both the Yadana (Fig. 6) and 3DF (Fig. 8) platforms. In addition, the demise of the 3DE Platform occurred concomitantly at the beginning of the Aquitanian (S4; Fig. 15c), suggesting that the rate of accommodation creation was superior to the growth rate potential of the carbonate platforms in the early

stages of the Miocene (Kendall and Schlager, 1981; Sarg, 1988; Schlager, 2005). These conditions led to (Fig. 15c): (1) regional backstepping of the Yadana and 3DF platforms; (2) transition from an attached to an isolated setting for the Yadana Platform; and (3) drowning of the 3DE Platform. The end of the seismic sequence S4 marks the onset of this rapid and large regional increase in accommodation creation.

The Late Chattian (S3; Fig. 15b) corresponds in this study to a period of major exposure (e.g. erosional truncation along the U2 seismic unconformity in the 3DF Platform; Fig. 8) and the development of a thick clastic sequence in the seaway between the YSP and YNP (S3) (Fig. 6). We interpret that a drop in relative sea-level at this time led to the demise of the carbonate platforms. This period of exposure was accompanied by the formation of sinkholes (e.g. Fig. 11) and potentially the development of a fluvial network on the YSP. This fluvial system is inferred to have transported sediment from the 3CA High to the interplatform seaway where accommodation space was available (Fig. 15b). In the upper part of S3, the growth of small buildups on the YSP shelf (Fig. 6) and the presence of reefs around the sinkholes (Figs. 11 and 15b) can be interpreted as transgressive deposits associated with the flooding of the platform at the end of S3; or as the result of higher stratigraphic order sea-level fluctuations during S3 repetitively flooding the shelf. Analogous flooding events have been documented in Quaternary carbonate systems (e.g. Saqab and Bourget, 2015; Courgeon et al., 2016). Similarly, numerous sinkhole features visible across the Yadana Platform suggest that seismic unconformity U6 constitutes a subaerial exposure surface. Sinkholes are also observed throughout seismic sequence S2 (e.g. 3DF Platform; Fig. 8) suggesting several periods of exposure during the Chattian.

The eustatic variations described by Miller et al. (2005, 2011) show a strong correlation with the interpreted regional stratigraphic events. During the Late Chattian (S3), at -25 Ma, a eustatic fall of about 50 m occurred, followed by a ~1 My period of eustatic

lowstand before the Oligocene - Miocene transition at -24 Ma (Miller et al., 2011). This long lasting sea-level fall can be linked to the emersion of platforms (U2 exposure event) and the development of the clastic sequence S3 (Fig. 15b). Although age control is poor for the Aquitanian sequences, the beginning of the Aquitanian is associated with a rapid sea-level rise (~40 m) (Miller et al., 2011). This rise in relative sea level can be linked to the rapid rate of accommodation creation and the subsequent backstepping observed on the Yadana Platform, as well as the drowning of the 3DE Platform at the end of S4 (Fig. 15c). For the remainder of the Aquitanian however, sea-levels display an overall negative (falling) trend, which does not appear to significantly influence carbonate accumulation. Although the exposure surface developed at the top of the Yadana Platform may have been formed during the ~15 My hiatus following the carbonate accumulation (Fig. 2), the eustatic curve shows a sea-level fall toward the end of the Aquitanian, consistent with emersion of the platform, followed by a sea-level rise during the Burdigalian which can be associated with the development of carbonates in the 3CA High area. During the Chattian, the sea-level curve displays several sea-level cycles, with the last fall corresponding to the exposure described along the seismic unconformity U2. These sea-level falls reach amplitudes ranging between 20 and 40 m (Miller et al., 2011) and could be linked with the periods of exposure interpreted within seismic sequence S2 (e.g. Fig. 8). The presence of reef flats on the eastern side of the 3DF Platforms (Fig. 15a) and the western side of the Yadana Platform might represent some imprints of these past sea-level cycles, as can be observed on some modern carbonate platforms (e.g. Glorieuses Archipelago; Jorry et al., 2016). The accumulation of hundreds of meters of carbonates (e.g. ~850 m in the 3DF Platform) is unlikely to be the result of eustasy alone. Subsidence was likely the main control on the creation of accommodation space and the subsequent accumulation of carbonate sediments. However, 2<sup>nd</sup> to 3<sup>rd</sup> order sea-level fluctuations were overprinted on the subsidence signal, strongly influencing the stratigraphic architecture of the carbonate

platforms (Fig. 15). When rapid sea-level fall is superimposed on a steady subsidence rate, accommodation may become negative leading to subaerial exposure of the platforms (e.g. sea-level fall during the Late Chattian; Fig. 14). Conversely, if a rapid sea-level rise overprints the subsidence signal, the positive accommodation rapidly increases which may impact the aggradational and / or retrogradational patterns of the carbonate platforms (e.g. km-scale backstepping stages and drowning of the 3DE Platform during the Aquitanian).

## 6.2. Carbonate platform dynamics

### 6.2.1. Volcanic ridge model

Different authors have classified carbonate platforms based on their tectonics (e.g. Fulthorpe and Schlanger, 1989; Wilson, 2002; Bosence, 2005), their facies (e.g. Wilson, 1975), their morphology (e.g. Read, 1985) or their ecology (e.g. Pomar, 2001; Pomar and Kendall, 2008). The carbonate platforms in this study can be classified as two main types: attached, and isolated (*sensu* Read, 1985). At a larger scale (basinal), different morphological and stratigraphic characteristics of these platforms allow their classification as “volcanic pedestal platforms” (*sensu* Bosence, 2005) namely; (1) thick (~300 to 850 m) aggrading and backstepping geometries; (2) high subsidence rates (accommodation space creation); (3) steep (~3 to 8°) flanks; (4) limited progradation; and (5) stratigraphic architecture influenced by eustatic variations. These observations contrast with those that can be made in an active convergent tectonic setting, especially for “island-arc carbonates” or “intra-arc settings” (Fulthorpe and Schlanger, 1989; Soja, 1996; Dorobek, 2008; Wilson, 2002; Wilson and Hall, 2010). These observations include: (1) rapid facies changes between thin carbonate deposits and thick volcanoclastic deposits; (2) unpredictable and variable rates of subsidence and uplift

due to various scales of tectonic deformation; and (3) periods of volcanic activity hindering the shallow-water carbonate factory, with production only active during periods of volcanic quiescence. In the study area, during the Late Oligocene - Early Miocene, the Yadana, 3DF and 3DE platforms are not interbedded with any thick volcanic deposits and are not associated with active faulting (Fig. 15). These observations therefore lie in contrast with the volcanic arc model previously suggested for the Yadana High (e.g. Morley, 2013; Racey and Ridd, 2015).

Globally, isolated carbonate platforms commonly develop on volcanic basement in volcanic ridge settings within mature oceans (Wilson, 2002; Bosence 2005). Modern and ancient examples (e.g. the Maldives; Purdy and Bertram, 1993) are well known. The volcanic basement of the platforms in this study could be interpreted as this style of mature volcanic ridge (Maldives type), matching the “volcanic pedestal platform” model of Bosence (2005).

In the case of the volcanic ridge scenario, questions remain on the presence of a paleorelief (3CA High). From regional observations, a valid hypothesis could be a tilting of the volcanic ridge westward (Fig. 16a), consistent with the observation that the 3DF Platform is thicker than the Yadana Platform (Fig. 4). This insight means that the 3DF Platform had more available space for carbonate accumulation. On the opposite side of the ridge, a relief emerged (3CA High) with the YSP forming an attached platform at the beginning of the carbonate depositional history (Fig. 16a). This interpretation is consistent with the presence of the Eocene carbonate ramp thinning toward the east on the 3DF Platform (Figs. 4 and 8).

#### 6.2.2. *Burman margin evolution*

The data presented here suggest that the previous model considering the Yadana basement as a volcanic arc (Morley, 2013; Racey and Ridd, 2015) is inappropriate. The lack

of subduction in the north part of the Andaman Sea (and as a consequence, the absence of volcanic arc) can be attributed to the high obliquity of the movement between the Indian plate and the Burman microplate (Fig. 1a), (Maurin and Rangin, 2009a; Rangin, 2012; Fig. 1a). The only volcanoes in the area are located in the south part of the Andaman Sea and were developed during the Quaternary (Chakraborty and Khan, 2009). Consequently, it is unlikely that a massive volcanic basement (Fig. 1c) was present in the Yadana area before the initiation of carbonate production during the Cenozoic.

To explain the development of the carbonate platforms on a volcanic ridge, and the change to the present-day back-arc setting (Fig. 1a), a new model for the geodynamic evolution of the Burman margin has to be considered. Introduced by Rangin (2012) and based on regional studies of the Burman margin (e.g. Maurin, 2009; Maurin and Rangin, 2009a, 2009b), an alternative model considers the Yadana substratum as a volcanic ridge created during the northward motion of the Indian plate above the Kerguelen island hotspot, parallel to the well-known Ninety East Ridge (Weis and Frey, 2002; Silva et al., 2013; Fig. 16b). As the Indian plate and Yadana Ridge moved northward, a carbonate ramp developed during the Late Eocene, which was followed by carbonate platforms during the Chattian and Aquitanian (Fig. 15). An inter-ridge basin (i.e. the M5 Basin, Fig. 1b) was located between the ridges and was fed by the paleo-Bengal fan. The large volume of Eocene to Early Miocene siliciclastic sediments in this basin (Fig. 1c) may have been responsible for the loading of the oceanic crust and subsequent tilting of the Yadana Ridge toward the west (Fig. 16a). During the Early Miocene, this extensive mass of rigid volcanics collided with the Eurasian plate, potentially docking along the subduction trench, obstructing the subduction, and leading to a subduction jump. Similar modern complex interactions are observed between the 90°E Ridge and the subduction trench (Subrahmanyam et al., 2008; Maurin, 2009; Maurin and Rangin, 2009b; Kumar et al., 2013). The ridge thus became integrated in the Burman microplate (Fig. 1a).

This jump induced three major events during the Early - Middle Miocene: (1) the inversion of the M5 Basin in the west (Figs. 1b-c); (2) a dextral strike-slip movement, which triggered the wide opening of the Moattama Basin in the east (Figs. 1b-c); and (3) the creation of a North - South gutter exploited by the Irrawaddy River which began to form a significant delta to the south (Fig. 1a). The volcanic activity on the 3CA paleorelief during the Aquitanian - Burdigalian could be considered as a reactivation of the volcanism along transform faults. Further geochemical analysis would need to be conducted to assess the exact origin and age of this volcanism.

This succession of events is interpreted to have led to the present-day structural configuration in the north part of the Andaman Sea (Fig. 1a), and may explain the origin and location of the poorly understood Alcock and Sewell Rises (Fig. 1a), which could correspond to relics of the Yadana Ridge. Similarly, the M8 High (Fig. 1c) could be considered as a direct continuation of the Yadana Ridge southward, with the development of shallow-water carbonate platforms on its top.

### *6.2.3. Impact of the new geodynamic evolution on the platform demise*

The platforms of the Yadana area were developed during the Late Oligocene and the Early Miocene. However, while other platforms in the Indo-Pacific region continued their development through the Middle Miocene (Wilson, 2008), growth of the Yadana platforms terminated during the Early Miocene. These shallow-marine platforms are onlapped and overlain by deep-marine facies (i.e. pro-delta shales) after a hiatus of ~15 My (Fig. 2). Thus, the stratigraphic surface at the top of the platforms (i.e. seismic unconformity U6) can be interpreted as a drowning unconformity (*sensu* Schlager, 1981, 1999). An emersion event is also inferred at the top of the Yadana Platform as evidenced by the presence of sinkholes (Fig.

12). However, numerous examples have been documented where a drowning unconformity is associated with subaerial exposure before drowning (Godet, 2013).

The causes of drowning of carbonate platforms have been widely debated in the literature (Schlager, 1981, 1989, 1998, 1999; Kendall and Schlager, 1981; Erlich et al., 1990, 1993; Godet, 2013). Drowning corresponds to a situation in which the rate of creation of accommodation space greatly exceeds the accumulation rate of carbonates. However, Schlager (1981) recognized that for healthy carbonate platforms with high accumulation rates (e.g. Miocene platforms; Fulthorpe and Schlanger, 1989), the demise cannot be simply the result of long-term geological processes (e.g. eustasy, subsidence) because they should be able to “keep-up”. Instead, he emphasized the potential role of short-term processes (e.g. environmental deterioration; Erlich et al., 1990, 1993) which may explain patterns of the platforms in the Yadana area. In this case, to explain major perturbations in the paleoenvironmental conditions, we infer a complex interplay between short-term regional processes (e.g. tectonics) and environmental parameters (e.g. oceanography).

In the Yadana area, drowning is interpreted to correlate with the timing of the subduction jump. It is inferred that the subduction jump triggered the inversion of both the M5 and Preparis Basins (Figs. 1b-c), resulting in uplift and subsequent erosion of ~2500 m of strata (Fig. 1c). Before the erosion of such a vast quantity of sediment, a paleorelief was created in the west part of the study area. This paleorelief may have had a potentially dramatic impact on carbonate production and accumulation by limiting access to the Indian Ocean and changing local paleoceanographic conditions (e.g. current, hydrodynamic regime, salinity; Pomar et al., 2004, 2012; Wilson, 2008, 2011; Lokier et al., 2009). Despite long-term eustatic fluctuations probably weakening carbonate platform growth around the Aquitanian – Burdigalian (through a high rate of accommodation space creation) (*see section 5.3.*), it is suggested that this regional tectonic event (subduction jump) profoundly altered

paleoenvironmental conditions in the region, ultimately leading to the drowning of the platforms at this time (Godet, 2013).

### 6.3. Analogy with the Maldives Archipelago

From the previous observations and interpretations, the Maldives carbonate system seems to constitute an analogue for some of the Late Oligocene - Early Miocene platforms presented in this study (i.e. Yadana, 3DF and 3DE platforms) in terms of location, dynamics, stratigraphy, geomorphology and controls. This modern carbonate system (~3 km thick) initiated in the Early Eocene over a Paleocene volcanic ridge formed by the La Reunion hotspot (Purdy and Bertram, 1993; Aubert and Droxler, 1996; Belopolsky and Droxler, 2003). Both the Maldives and the platforms of the Yadana area were thus developed as volcanic pedestal platforms (*sensu* Bosence, 2005). Additionally, unlike previous studies suggesting a different tectonic context for the Yadana area (e.g. Mitra, 2005; Morley, 2013), the two systems were located in the Indian Ocean during the Late Oligocene - Early Miocene (Fig. 16b).

Similar to the Yadana Platform studied here, extensional tectonic events had an impact on the ~55 My old basement of the Maldives (i.e. presence of graben and horst structures) and thus on the location / development of the platforms and seaways (Purdy and Bertram, 1993; Aubert and Droxler, 1996; Belopolsky and Droxler, 2003). The Maldives host a thin Eocene carbonate ramp (Fig. 16c) dominated by a large benthic foraminifera biota (Aubert and Droxler, 1996) that could be compared to the Upper Eocene carbonate ramp identified in the 3DF Platform (Figs. 8 and 16d). Following this, thick aggradational Late Oligocene - Early Miocene carbonate platforms are developed in both cases (Fig. 16c and 16d). However, the

Maldives differ in that they show a substantial thickness of Lower Oligocene carbonates (Fig. 16c), which are not observed in the Yadana area (Fig. 16d).

The platforms presented in this paper show similarities with the Maldives platforms during the Late Oligocene - Early Miocene. Both the Yadana area and the Maldives present thick (up to 1 km) aggrading platforms (e.g. 3DF Platform and west Maldives platform; Figs. 16c and 16d) and small-scale (between ~5 and 10 km) buildups developed on paleotopographic highs that halted their growth prematurely (e.g. 3DE Platform and buildup in the East part of the Maldives; Figs. 16c and 16d). However, attached features are noticeably absent in the Maldives where no such tilting is present. This constitutes an important contrast between the two systems.

Similarly to the Yadana area, the accumulation of hundreds of meters of carbonates in the Maldives during the Late Oligocene - Early Miocene was mainly driven by the subsidence of the volcanic ridge creating accommodation space (Betzler et al., 2013). Moreover, the study of the stratigraphic architecture of both systems leads to the interpretation of a strong eustatic influence (Purdy and Bertram, 1993; Aubert and Droxler, 1996; Belopolsky, 2000; Belopolsky and Droxler, 2003, 2004; Betzler et al., 2013). For example, two transgressive megasequences during the Late Oligocene and Early Miocene (Figs. 15a and 15c); a sea-level fall around the Oligocene - Miocene boundary (Fig. 15b); kilometer-scale backstepping events; and the drowning of small buildups during the Early Miocene (Fig. 15c).

These similarities emphasize that global (e.g. eustasy, climate) and local (e.g. oceanographic) conditions in the Indian Ocean were suitable for the development of thick and widespread carbonate systems during the Late Oligocene - Early Miocene. However, while the Maldives continued their development during the Middle Miocene (mainly influenced by strong currents) (Betzler et al., 2009, 2013; Lüdmann et al., 2013), carbonate growth ceased in the Yadana area. This observation is consistent with the interpretation of regional tectonic

events leading to the demise of the Yadana platforms through significant changes in the paleoenvironmental conditions.

## 7. Conclusion

A combination of 2D and 3D seismic (seismic facies, attribute analysis) combined with well data (sedimentary facies) allowed the regional paleogeographical reconstruction of attached and isolated platforms which developed over a volcanic basement in the Yadana area (Andaman Sea, offshore Myanmar) through the Late Oligocene - Early Miocene. In conjunction with favorable environmental conditions (e.g. oceanography, climate), subsidence was the main control on the creation of accommodation space leading to the accumulation of thick intervals of shallow-water carbonates (~300 to 850 m). 2<sup>nd</sup> to 3<sup>rd</sup> order eustatic fluctuations played a key role in the evolution of this carbonate depositional system through time and space, by impacting regionally the stratigraphic architecture of the platforms (i.e. development of regional stratigraphic surfaces and sequences), which can be summarised in three main stages.

Firstly, four carbonate platforms initiated during the Chattian: the 3DF Platform, 3DE Platform, Yadana North Platform (YNP) and Yadana South Platform (YSP), the latter being the only attached platform. A regional westward tilt created local differential subsidence allowing the accumulation of thicker carbonates in the 3DF Platform, while uplift formed relief (the 3CA High) in the east, allowing the YSP platform to assume an attached configuration. A minor input of clastic sediments was then supplied to the system without dramatically impacting carbonate production. Secondly, a drop in the sea-level led to the emersion of all the platforms at the end of the Chattian, resulting in extensive karstification. The development of a drainage system is also inferred on the YSP, leading to the deposition

of a thick progradational clastic package in the interplatform seaway between the YNP and the YSP, with sediments probably sourced from the adjacent 3CA High. Thirdly, upon resumption of carbonate production, a rapid sea-level rise at the beginning of the Aquitanian triggered km-scale backstepping on the large platforms, while the smaller platform (3DE Platform) was drowned. For the Yadana Platform (now reinitiated as one large platform), this period represents the transition from an attached to an isolated configuration. The Aquitanian marks as well the onset of renewed volcanic activity on the 3CA High, leading to the formation of thick volcanic deposits in the east, followed by the development of fringing reefs and isolated carbonate buildups during the Burdigalian.

The stratigraphic observations and associated interpretations concerning the controlling parameters on carbonate development in this study are largely incompatible with any previous geodynamic models (i.e. a volcanic arc) as the basement for this carbonate system. Instead, using an alternative geodynamic model for the Burman margin evolution, we infer that the carbonate platforms documented here were developed on a volcanic ridge of hotspot origin (Kerguelen) in the Indian Ocean. A comparison with the Late Oligocene - Early Miocene carbonate platforms from the Maldives Archipelago, interpreted to be developed in the same geographic and environmental setting, displays similarities with the carbonate platforms of the Yadana area, including: thick carbonates (hundreds of meters), extended size (tens of kilometers), stratigraphic patterns (two transgressive megasequences represented by aggrading carbonate strata during Chattian and Aquitanian respectively), and long-term controlling parameters on carbonate accumulation (subsidence and eustasy). This highlights that paleogeographical and paleoenvironmental conditions in the Indian Ocean were highly favorable for the carbonate depositional systems to thrive regionally at this time. However, a large-scale tectonic event along the Burman margin (i.e. subduction jump) created a paleorelief (~2 km of uplift) in the west part of the Yadana area, which locally modified the

paleoenvironmental conditions (e.g. oceanography). This dramatic change is interpreted to be a key factor leading to the drowning and ultimate demise of the Yadana carbonate depositional system. The sudden death of the Yadana carbonate platforms occurred during a time regarded as highly favourable for carbonate production in the Indo-Pacific region, and whilst the Yadana system succumbed, the Maldives continued their development throughout the Middle Miocene. Hence, the Yadana area constitutes a good example for the understanding of the complex relationships between global and local mechanisms on carbonate platform initiation, growth and demise.

### **Acknowledgments**

The authors would like to thank Total E&P which has provided all the financial support to realize this project and has authorized the publication of this paper, as well as the different partners: Chevron, Petroleum Authority of Thailand Exploration (PTTEP), and Myanmar Oil and Gas Enterprise (MOGE). We also thank Total E&P Myanmar for providing the seismic and well data. We are also indebted to Gene Rankey and an anonymous reviewer for their very detailed and insightful comments, which significantly improve the quality of this manuscript. We are particularly grateful to Tom Wilson for improving the english of the last version of the manuscript. We thank as well Sven Egenhoff (Associate Editor) for his help on this submission. We are grateful to all the following persons for their technical support and wise advices: Franck Gisquet, Christophe Matonti, Thomas Teillet, Bruno Caline, Loic Richard, Laurent Guy, Fei Hong, Céline Barberan, Ronan Petton, Aurelien Vigorne and all the other persons who have participated in the study of Yadana throughout the years. We thank as well Pascal Barrier and Cyril Gagnaison (Institut Polytechnique LaSalle Beauvais) for their preliminary remarks on the results.

**REFERENCES**

- Aubert, O., Droxler, A.W., 1996. Seismic stratigraphy and depositional signatures of the Maldives carbonate system (Indian Ocean). *Marine and Petroleum Geology* 13, 503–536.
- Bachtel, S.L., Kissling, R.D., Martrono, D., Rahardjanto, S.P., Dunn, P.A., MacDonald, B.A., 2004. Seismic stratigraphic evolution of the Miocene-Pliocene Segitiga Platform, East Natuna Sea, Indonesia: the origin, growth, and demise of an isolated carbonate platform, in: Eberli, G.P., Masafarro, J.L., Sarg, J.F. (Eds.), *Seismic Imaging of Carbonate Reservoirs and Systems*. AAPG Memoir 81, pp. 309–328.
- Belopolsky, A., Droxler, A., 2003. Imaging Tertiary carbonate system-the Maldives, Indian Ocean: Insights into carbonate sequence interpretation. *The Leading Edge* 22, 646–652.
- Belopolsky, A.V., 2000. Tectonic and eustatic controls on the evolution of the maldive carbonate platform. Rice University.
- Belopolsky, A. V., Droxler, A.W., 2004. Seismic expressions of prograding carbonate bank margins: Middle Miocene, Maldives, Indian Ocean, in: Eberli, G.P., Masafarro, J.L., Sarg, J.F. (Eds.), *Seismic Imaging of Carbonate Reservoirs and Systems*. AAPG Memoir 81, pp. 267–290.
- Betzler, C., Fürstenau, J., Lüdmann, T., Hübscher, C., Lindhorst, S., Paul, A., Reijmer, J.J.G., Droxler, A.W., 2013. Sea-level and ocean-current control on carbonate-platform growth, Maldives, Indian Ocean. *Basin Research* 25, 172–196. doi:10.1111/j.1365-2117.2012.00554.x

- Betzler, C., Hübscher, C., Lindhorst, S., Reijmer, J.J.G., Römer, M., Droxler, A.W., Fürstenau, J., Lüdmann, T., 2009. Monsoon-induced partial carbonate platform drowning (Maldives, Indian Ocean). *Geology* 37, 867–870. doi:10.1130/G25702A.1
- Borgomano, J.R.F., Fournier, F., Viseur, S., Rijkels, L., 2008. Stratigraphic well correlations for 3-D static modeling of carbonate reservoirs. *AAPG Bulletin* 92, 789–824. doi:10.1306/02210807078
- Bosence, D., 2005. A genetic classification of carbonate platforms based on their basinal and tectonic settings in the Cenozoic. *Sedimentary Geology* 175, 49–72. doi:10.1016/j.sedgeo.2004.12.030
- Bubb, J.N., Hatlelid, W.G., 1977. Seismic stratigraphy and global changes of sea level, part 10: seismic recognition of carbonate build-ups, in: Payton, C.E. (Ed.), *Seismic Stratigraphy - Applications to Hydrocarbon Exploration*. AAPG Memoir 26, pp. 185–204.
- Burgess, P.M., Winefield, P., Minzoni, M., Elders, C., 2013. Methods for identification of isolated carbonate buildups from seismic reflection data. *AAPG Bulletin* 97, 1071–1098. doi:10.1306/12051212011
- Chakraborty, P.P., Khan, P.K., 2009. Cenozoic geodynamic evolution of the Andaman-Sumatra subduction margin: Current understanding. *Island Arc* 18, 184–200. doi:10.1111/j.1440-1738.2008.00643.x
- Chopra, S., Marfurt, K.J., 2007. Seismic attributes for prospect identification and reservoir characterization. *SEG Geophysical Developments Series* 11.

- Courgeon, S., Bourget, J., Jorry, S.J., 2016. A Pliocene-Quaternary analogue for ancient epeiric carbonate settings: The Malita intrashelf basin (Bonaparte Basin, northwest Australia). *AAPG Bulletin* 100, 565–595. doi:10.1306/02011613196
- Curry, J.R., 2005. Tectonics and history of the Andaman Sea region. *Journal of Asian Earth Sciences* 25, 187–232. doi:10.1016/j.jseas.2004.09.001
- Curry, J.R., Moore, D.G., Lawver, L.A., Emmel, F.J., Raitt, R.W., Henry, M., Kieckhefer, R., 1979. Tectonics of the Andaman Sea and Burma, in: Watkins, J., Montadert, L., Dickinson, P.W. (Eds.), *Geological and Geophysical Investigations of Continental Margins*. AAPG Memoir 29, pp. 189–198.
- Dorobek, S.L., 2008. Carbonate-platform facies in volcanic arc settings: Characteristics and controls on deposition and stratigraphic development, in: Draut, A.E., Clift, P.D., Scholl, D.W. (Eds.), *Formation and Applications of the Sedimentary Record in Arc Collision Zones*. Geological Society of America Special Paper 436, pp. 55–90.
- Droxler, A.W., Jorry, S.J., 2013. Deglacial origin of barrier reefs along low-latitude mixed siliciclastic and carbonate continental shelf edges. *Annual Review of Marine Science* 5, 165–190. doi:10.1146/annurev-marine-121211-172234
- Epting, M., 1980. Sedimentology of Miocene carbonate buildups, Central Luconia, offshore Sarawak. *Geological Society of Malaysia Bulletin* 12, 17–30.
- Epting, M., 1989. Miocene carbonate buildups of Central Luconia, offshore Sarawak, in: Bally, A.W. (Ed.), *Atlas of Seismic Stratigraphy 3*. AAPG Studies in Geology 27, pp. 168–173.

- Erlich, E.N., Barrett, S.F., Ju, G.B., 1990. Seismic and geologic characteristics of drowning events on carbonate platforms. *AAPG Bulletin* 74, 1523–1537.
- Erlich, E.N., Longo, A.P., Hyate, S., 1993. Response of carbonate platform margins to drowning: evidence of environmental collapse, in: Loucks, R.G., Sarg, J.F. (Eds.), *Carbonate Sequence Stratigraphy: Recent Developments and Applications*. AAPG Memoir 57, pp. 241–266.
- Fournier, F., Borgomano, J., 2007. Geological significance of seismic reflections and imaging of the reservoir architecture in the Malampaya gas field (Philippines). *AAPG Bulletin* 91, 235–258. doi:10.1306/10160606043
- Fournier, F., Borgomano, J., Montaggioni, L.F., 2005. Development patterns and controlling factors of Tertiary carbonate buildups: Insights from high-resolution 3D seismic and well data in the Malampaya gas field (Offshore Palawan, Philippines). *Sedimentary Geology* 175, 189–215. doi:10.1016/j.sedgeo.2005.01.009
- Fournier, F., Montaggioni, L., Borgomano, J., 2004. Paleoenvironments and high-frequency cyclicity from Cenozoic South-East Asian shallow-water carbonates: a case study from the Oligo-Miocene buildups of Malampaya (Offshore Palawan, Philippines). *Marine and Petroleum Geology* 21, 1–21. doi:10.1016/j.marpetgeo.2003.11.012
- Fulthorpe, C.S., Schlanger, S.O., 1989. Paleo-oceanographic and tectonic settings of Early Miocene reefs and associated carbonates of offshore Southeast Asia. *AAPG Bulletin* 73, 729–756.

- Godet, A., 2013. Drowning unconformities: Palaeoenvironmental significance and involvement of global processes. *Sedimentary Geology* 293, 45–66. doi:10.1016/j.sedgeo.2013.05.002
- Greenlee, S.M., Lehmann, P.J., 1993. Stratigraphic framework of productive carbonate buildups, in: Loucks, R.G., Sarg, J.F. (Eds.), *Carbonate Sequence Stratigraphy: Recent Developments and Applications*. AAPG Memoir 57, pp. 43–62.
- Grötsch, J., Mercadier, C., 1999. Integrated 3D reservoir modeling based on 3D seismic: the Tertiary Malampaya and Camago buildups, offshore Palawan, Philippines. *AAPG Bulletin* 83, 1703–1728.
- Hall, R., 1998. The plate tectonics of Cenozoic SE Asia and the distribution of land and sea, in: Hall, R., Holloway, J.D. (Eds.), *Biogeography and Geological Evolution of SE Asia*. pp. 99–131.
- Hall, R., 2002. Cenozoic geological and plate tectonic evolution of SE Asia and the SW Pacific: computer-based reconstructions, model and animations. *Journal of Asian Earth Sciences* 20, 353–431.
- Hall, R., 2012. Late Jurassic–Cenozoic reconstructions of the Indonesian region and the Indian Ocean. *Tectonophysics* 570–571, 1–41. doi:10.1016/j.tecto.2012.04.021
- Hallock, P., 2005. Global change and modern coral reefs: New opportunities to understand shallow-water carbonate depositional processes 175, 19–33. doi:10.1016/j.sedgeo.2004.12.027
- Handford, C.R., Loucks, R.G., 1993. Carbonate depositional sequences and systems tracts - Responses of carbonate platforms to relative sea-level changes, in: Loucks, R.G., Sarg,

- J.F. (Eds.), Carbonate Sequence Stratigraphy: Recent Developments and Applications. AAPG Memoir 57, pp. 3–41.
- Jordan, C.F., Abdullah, M., 1992. Arun Field - Indonesia, Norh Sumatra Basin, Indonesia, in: Foster, N.H., Beaumont, E.A. (Eds.), Stratigraphic Traps III. AAPG Treatise of petroleum geology, atlas of oil and gas fields, pp. 1–39.
- Jorry, S.J., Camoin, G.F., Jouet, G., Roy, P. Le, Vella, C., Courgeon, S., Prat, S., Fontanier, C., Paumard, V., Boulle, J., Caline, B., Borgomano, J., 2016. Modern sediments and Pleistocene reefs from isolated carbonate platforms (Iles Eparses, SW Indian Ocean): A preliminary study. *Acta Oecologica* 72, 129–143. doi:10.1016/j.actao.2015.10.014
- Kamesh Raju, K.A., Ramprasad, T., Rao, P.S., Ramalingeswara Rao, B., Varghese, J., 2004. New insights into the tectonic evolution of the Andaman basin, northeast Indian Ocean. *Earth and Planetary Science Letters* 221, 145–162. doi:10.1016/S0012-821X(04)00075-5
- Kendall, C.G., Schlager, W., 1981. Carbonates and relative changes in sea-level. *Marine Geology* 44, 181–212.
- Khan, P.K., Chakraborty, P.P., 2005. Two-phase opening of Andaman Sea: a new seismotectonic insight. *Earth and Planetary Science Letters* 229, 259–271. doi:10.1016/j.epsl.2004.11.010
- Koša, E., 2015. Sea-level changes, shoreline journeys, and the seismic stratigraphy of Central Luconia, Miocene-present, offshore Sarawak, NW Borneo. *Marine and Petroleum Geology* 59, 35–55. doi:10.1016/j.marpetgeo.2014.07.005

- Koša, E., Warrlich, G.M.D., Loftus, G., 2015. Wings, mushrooms, and Christmas trees: The carbonate seismic geomorphology of Central Luconia, Miocene–present, offshore Sarawak, northwest Borneo. *AAPG Bulletin* 99, 2043–2075. doi:10.1306/06181514201
- Kumar, R.T.R., Windley, B.F., Rajesh, V.J., Santosh, M., 2013. Elastic thickness structure of the Andaman subduction zone: Implications for convergence of the Ninetyeast Ridge. *Journal of Asian Earth Sciences* 78, 291–300. doi:10.1016/j.jseaes.2013.01.018
- Kusumastuti, A., Van Rensbergen, P., Warren, J.K., 2002. Seismic sequence analysis and reservoir potential of drowned Miocene carbonate platforms in the Madura Strait, East Java, Indonesia. *AAPG Bulletin* 86, 213–232.
- Le Roy, P., Cabioch, G., Monod, B., Lagabrielle, Y., Pelletier, B., Flamand, B., 2008. Late Quaternary history of the Nouméa lagoon (New Caledonia, South West Pacific) as depicted by seismic stratigraphy and multibeam bathymetry - A modern model of tropical rimmed shelf. *Palaeogeography, Palaeoclimatology, Palaeoecology* 270, 29–45. doi:10.1016/j.palaeo.2008.08.012
- Lee, T.-Y., Lawver, L.A., 1995. Cenozoic plate reconstruction of Southeast Asia. *Tectonophysics* 251, 85–138. doi:10.1016/0040-1951(95)00023-2
- Lokier, S.W., Wilson, M.E.J., Burton, L.M., 2009. Marine biota response to clastic sediment influx: A quantitative approach. *Palaeogeography, Palaeoclimatology, Palaeoecology* 281, 25–42. doi:10.1016/j.palaeo.2009.07.007
- Lüdmann, T., Kalvelage, C., Betzler, C., Fürstenau, J., Hübscher, C., 2013. The Maldives, a giant isolated carbonate platform dominated by bottom currents. *Marine and Petroleum Geology* 43, 326–340. doi:10.1016/j.marpetgeo.2013.01.004

- Lukasik, J., Simo, J.A., 2008. Controls on development of Phanerozoic carbonate platforms and reefs - Introduction and synthesis, in: Lukasik, J., Simo, J.A. (Eds.), Controls on Carbonate Platform and Basin Development. SEPM Special Publication 89, pp. 5–12.
- Masaferro, J.L., Bourne, R., Jauffred, J.C., 2004. Three-dimensional seismic volume visualization of carbonate reservoirs and structures, in: Eberli, G.P., Masaferro, J.L., Sarg, J.F. (Eds.), Seismic Imaging of Carbonate Reservoirs and Systems. AAPG Memoir 81, pp. 11–41.
- Maurin, T., 2009. 90°E ridge and East-Tibetan crustal flow impact on the recent evolution of the Indo-Burmese oblique subduction. Universite Paul Cezanne.
- Maurin, T., Rangin, C., 2009a. Structure and kinematics of the Indo-Burmese Wedge: Recent and fast growth of the outer wedge. *Tectonics* 28, 1–21. doi:10.1029/2008TC002276
- Maurin, T., Rangin, C., 2009b. Impact of the 90°E ridge at the Indo-Burmese subduction zone imaged from deep seismic reflection data. *Marine Geology* 266, 143–155. doi:10.1016/j.margeo.2009.07.015
- Menier, D., Pierson, B., Chalabi, A., Ting, K.K., Pubellier, M., 2014. Morphological indicators of structural control, relative sea-level fluctuations and platform drowning on present-day and Miocene carbonate platforms. *Marine and Petroleum Geology* 58, 776–788. doi:10.1016/j.marpetgeo.2014.01.016
- Miller, K.G., Kominz, M.A., Browning, J. V., Wright, J.D., Mountain, G.S., Katz, M.E., Sugarman, P.J., Cramer, B.S., Christie-Blick, N., Pekar, S.F., 2005. The Phanerozoic record of global sea-level change. *Science* 310, 1293–1298. doi:10.1126/science.1116412

- Miller, K.G., Mountain, G.S., Wright, J.D., Browning, J. V., 2011. Sea level and ice volume variations from continental margin and deep-sea isotopic records. *Oceanography* 24, 40–53. doi:10.5670/oceanog.2011.26.COPYRIGHT
- Mitchum, R.M., Vail, P.R., Sangree, J.B., 1977a. Seismic stratigraphy and global changes of sea-level, part 6: stratigraphic interpretation of seismic reflection patterns in depositional sequences, in: Payton, C.E. (Ed.), *Seismic Stratigraphy - Applications to Hydrocarbon Exploration*. AAPG Memoir 26, pp. 117–133.
- Mitchum, R.M., Vail, P.R., Thompson, S., 1977b. Seismic stratigraphy and global changes of sea-level, part 2: the depositional sequence as a basic unit for stratigraphic analysis, in: Payton, C.E. (Ed.), *Seismic Stratigraphy - Applications to Hydrocarbon Exploration*. AAPG Memoir 26, pp. 53–62.
- Mitra, D., 2005. Late Oligocene and Miocene evolution of the carbonate system in the Gulf of Martaban (Northern Andaman Sea): effects of eustacy, tectonics, and siliciclastic input, comparison with the Maldives carbonate system. Rice University.
- Morley, C.K., 2002. A tectonic model for the Tertiary evolution of strike-slip faults and rift basins in SE Asia. *Tectonophysics* 347, 189–215. doi:10.1016/S0040-1951(02)00061-6
- Morley, C.K., 2012. Late Cretaceous-Early Palaeogene tectonic development of SE Asia. *Earth-Science Reviews* 115, 37–75. doi:10.1016/j.earscirev.2012.08.002
- Morley, C.K., 2013. Discussion of tectonic models for Cenozoic strike-slip fault-affected continental margins of mainland SE Asia. *Journal of Asian Earth Sciences* 76, 137–151. doi:10.1016/j.jseaes.2012.10.019

- Neuhaus, D., Borgomano, J., Jauffred, J.-C., Mercadier, C., Olotu, S., Grötsch, J., 2004. Quantitative seismic reservoir characterization of an Oligocene-Miocene carbonate buildup: Malampaya field, Philippines, in: Eberli, G.P., Masafarro, J.L., Sarg, J.F. (Eds.), *Seismic Imaging of Carbonate Reservoirs and Systems*. AAPG Memoir 81, pp. 169–183.
- Pickering, K.T., Hiscott, R.N., Hein, F.J., 1989. *Deep-marine Environments: Clastic Sedimentation and Tectonics*.
- Pomar, L., 2001. Types of carbonate platforms: a genetic approach. *Basin Research* 13, 313–334.
- Pomar, L., Bassant, P., Brandano, M., Ruchonnet, C., Janson, X., 2012. Impact of carbonate producing biota on platform architecture: Insights from Miocene examples of the Mediterranean region. *Earth-Science Reviews* 113, 186–211. doi:10.1016/j.earscirev.2012.03.007
- Pomar, L., Kendall, C.G.S.C., 2008. Architecture of carbonate platforms: a response to hydrodynamics and evolving ecology, in: Lukasik, J., Simo, J.A. (Eds.), *Controls on Carbonate Platform and Basin Development*. SEPM Special Publication 89, pp. 187–216.
- Posamentier, H.W., Laurin, P., Warmath, A., Purnama, M., Drajat, D., 2010. Seismic stratigraphy and geomorphology of Oligocene to Miocene carbonate buildups, offshore Madura, Indonesia, in: Morgan, W.A., George, A.D., Harris, P.M., Kupecz, J.A., Sarg, J.F. (Eds.), *Cenozoic Carbonate Systems of Australasia*. SEPM Special Publication 95, pp. 175–192.

- Prat, S., Jorry, S.J., Jouet, G., Camoin, G., Vella, C., Le, P., Caline, B., Boichard, R., Pastol, Y., 2016. Geomorphology and sedimentology of a modern isolated carbonate platform: The Glorieuses archipelago, SW Indian Ocean. *Marine Geology* 380, 272–283. doi:10.1016/j.margeo.2016.04.009
- Purdy, E.G., Bertram, G.T., 1993. Carbonate concepts from the Maldives, Indian Ocean. *AAPG Studies in Geology* 34.
- Racey, A., Ridd, M.F., 2015. Petroleum geology of the Moattama Region, Myanmar, in: Racey, A., Ridd, M.F. (Eds.), *Petroleum Geology of Myanmar*. Geological Society of London Memoir 45, pp. 63–81.
- Radhakrishna, M., Lasitha, S., Mukhopadhyay, M., 2008. Seismicity, gravity anomalies and lithospheric structure of the Andaman arc, NE Indian Ocean. *Tectonophysics* 460, 248–262. doi:10.1016/j.tecto.2008.08.021
- Rangin, C., 2012. Cenozoic geodynamic evolution of the Burma-Andaman platelet. *AAPG Search and Discovery Article* 30258.
- Read, J.F., 1985. Carbonate platform facies models. *AAPG Bulletin* 69, 1–21.
- Rudolph, K.W., Lehmann, P.J., 1989. Platform evolution and sequence stratigraphy of the Natuna Platform, South China Sea, in: Crevello, P.D., Wilson, J.L., Sarg, J.F., Read, J.F. (Eds.), *Controls on Carbonate Platform and Basin Development*. SEPM Special Publication 44, pp. 353–361.
- Saller, A.H., Vijaya, S., 2002. Depositional and diagenetic history of the Kerendan carbonate platform, Oligocene, Central Kalimantan, Indonesia. *Journal of Petroleum Geology* 25, 123–150.

- Saqab, M.M., Bourget, J., 2015. Controls on the distribution and growth of isolated carbonate build-ups in the Timor Sea (NW Australia) during the Quaternary. *Marine and Petroleum Geology* 62, 123–143. doi:10.1016/j.marpetgeo.2015.01.014
- Sarg, J.F., 1988. Carbonate sequence stratigraphy, in: Wilgus, C.K., Hastings, B.S., Kendall, C.G.S.C., Posamentier, H.W., Ross, C.A., Van Wagoner, J.C. (Eds.), *Sea-Level Changes: An Integrated Approach*. SEPM Special Publication 42, pp. 155–181. doi:10.2110/pec.88.01.0155
- Schlager, W., 1981. The paradox of drowned reefs and carbonate platforms. *Geological Society of America Bulletin* 92, 197–211.
- Schlager, W., 1989. Drowning unconformities on carbonate platforms, in: Crevello, P.D., Wilson, J.L., Sarg, J.F., Read, J.F. (Eds.), *Controls on Carbonate Platform and Basin Development*. SEPM Special Publication 44, pp. 15–25.
- Schlager, W., 1998. Exposure, drowning and sequence boundaries on carbonate platforms, in: Camoin, G.F., Davies, P.J. (Eds.), *Reefs and Carbonate Platforms in the Pacific and Indian Oceans*. International Association of Sedimentologists Special Publication 25, pp. 3–21. doi:10.1016/S0264-8172(00)00056-8
- Schlager, W., 1999. Type 3 sequence boundaries, in: Harris, P.M., Saller, A.H., Simo, J.A. (Eds.), *Advances in Carbonate Sequence Stratigraphy: Application to Reservoirs, Outcrops and Models*. SEPM Special Publication 63, pp. 35–45.
- Schlager, W., 2005. Carbonate sedimentology and sequence stratigraphy. *SEPM Concepts in Sedimentology and Paleontology* 8. doi:10.2110/csp.05.08

- Silva, I.G.N., Weis, D., Scoates, J.S., Barling, J., 2013. The Ninetyeast Ridge and its relation to the Kerguelen, Amsterdam and St. Paul hotspots in the Indian Ocean. *Journal of Petrology* 54, 1177–1210. doi:10.1093/petrology/egt009
- Soja, C., 1996. Island-arc carbonates: characterization and recognition in the ancient geologic record. *Earth-Science Reviews* 41, 31–65. doi:10.1016/0012-8252(96)00029-3
- Subrahmanyam, C., Gireesh, R., Chand, S., Kamesh Raju, A.K., Rao, D.G., 2008. Geophysical characteristics of the Ninetyeast Ridge–Andaman island arc/trench convergent zone. *Earth and Planetary Science Letters* 266, 29–45. doi:10.1016/j.epsl.2007.10.016
- Tucker, M.E., Wright, V.P., 1990. *Carbonate Sedimentology*. Blackwell Publishing Ltd., Oxford, UK. doi:10.1002/9781444314175
- Vahrenkamp, V.C., David, F., Duijndam, P., Newall, M., Crevello, P., 2004. Growth architecture, faulting, and karstification of a Middle Miocene carbonate platform, Luconia province, offshore Sarawak, Malaysia, in: Eberli, G.P., Masafarro, J.L., Sarg, J.F. (Eds.), *Seismic Imaging of Carbonate Reservoirs and Systems*. AAPG Memoir 81, pp. 329–350.
- Vail, P.R., Mitchum, R.M., 1977. Seismic stratigraphy and global changes of sea-level, part 1: overview, in: Payton, C.E. (Ed.), *Seismic Stratigraphy - Applications to Hydrocarbon Exploration*. AAPG Memoir 26, pp. 51–52.
- Weis, D., Frey, F.A., 2002. Submarine basalts of the northern Kerguelen Plateau: Interaction between the Kerguelen Plume and the Southeast Indian Ridge revealed at ODP Site 1140. *Journal of Petrology* 43, 1287–1309. doi:10.1093/petrology/43.7.1287

- Wilson, J.L., 1975. Carbonate facies in geologic history.
- Wilson, M.E.J., 2000. Tectonic and volcanic influences on the development and diachronous termination of a tertiary tropical carbonate platform. *Journal of Sedimentary Research* 70, 310–324.
- Wilson, M.E.J., 2002. Cenozoic carbonates in Southeast Asia: implications for equatorial carbonate development. *Sedimentary Geology* 147, 295–428. doi:10.1016/S0037-0738(01)00228-7
- Wilson, M.E.J., 2008. Global and regional influences on equatorial shallow-marine carbonates during the Cenozoic. *Palaeogeography, Palaeoclimatology, Palaeoecology* 265, 262–274. doi:10.1016/j.palaeo.2008.05.012
- Wilson, M.E.J., 2011. SE Asian carbonates: tools for evaluating environmental and climatic change in equatorial tropics over the last 50 million years, in: Hall, R., Cottam, M. A., Wilson, M.E.J. (Eds.), *The SE Asian Gateway: History and Tectonics of the Australia-Asia Collision*. Geological Society of London Special Publication 355, pp. 347–372. doi:10.1144/SP355.18
- Wilson, M.E.J., Hall, R., 2010. Tectonic influences on SE Asian carbonate systems and their reservoir development, in: Morgan, W.A., George, A.D., Harris, P.M., Kupecz, J.A., Sarg, J.F. (Eds.), *Cenozoic Carbonate Systems of Australasia*. SEPM Special Publication 95, pp. 13–40.
- Wilson, M.E.J., Lokier, S.W., 2002. Siliciclastic and volcanoclastic influences on equatorial carbonates: insights from the Neogene of Indonesia. *Sedimentology* 49, 583–601.

- Woolfe, K.J., Naish, T., Purdon, R.G., 1998. Lowstand rivers need not incise the shelf: An example from the Great Barrier Reef, Australia, with implications for sequence stratigraphic models. *Geology* 26, 75–78.
- Zampetti, V., 2010. Controlling factors of a Miocene carbonate platform: implications for platform architecture and off-platform reservoirs (Luconia province, Malaysia), in: Morgan, W.A., George, A.D., Harris, P.M., Kupecz, J.A., Sarg, J.F. (Eds.), *Cenozoic Carbonate Systems of Australasia*. SEPM Special Publication 95, pp. 129–145.
- Zampetti, V., Schlager, W., Konijnenburg, J.-H., Everts, A.-J., 2004a. 3-D seismic characterization of submarine landslides on a Miocene carbonate platform (Luconia province, Malaysia). *Journal of Sedimentary Research* 74, 817–830. doi:10.1306/040604740817
- Zampetti, V., Schlager, W., van Konijnenburg, J.-H., Everts, A.-J., 2004b. Architecture and growth history of a Miocene carbonate platform from 3D seismic reflection data; Luconia province, offshore Sarawak, Malaysia. *Marine and Petroleum Geology* 21, 517–534. doi:10.1016/j.marpetgeo.2004.01.006

Fig. 1.

(A) Simplified tectonic map of the Andaman Sea region (after [Morley, 2002](#), 2012b; [Kamesh Raju et al., 2004](#) and [Curray, 2005](#)). The Late Oligocene - Early Miocene platforms are located beneath the Myanmar continental shelf. (B) Base seal depth-structure map (bold contours are every 500 m) interpreted from regional 2D seismic data. The upper map indicates the basins, highs and wells location; the lower map presents the dataset of this study with regional 2D seismic and one 3D seismic volume located on the Yadana gas field. (C) Interpreted regional 2D seismic profile through the Yadana area (see location on B) showing the main lithostratigraphic units of the area with their relative geologic age. There is a hiatus of ~15 My between the top of the carbonates and the Upper Miocene shales (regional seal). The eastward tilt explains the trap creation in the west part of the Yadana Platform.

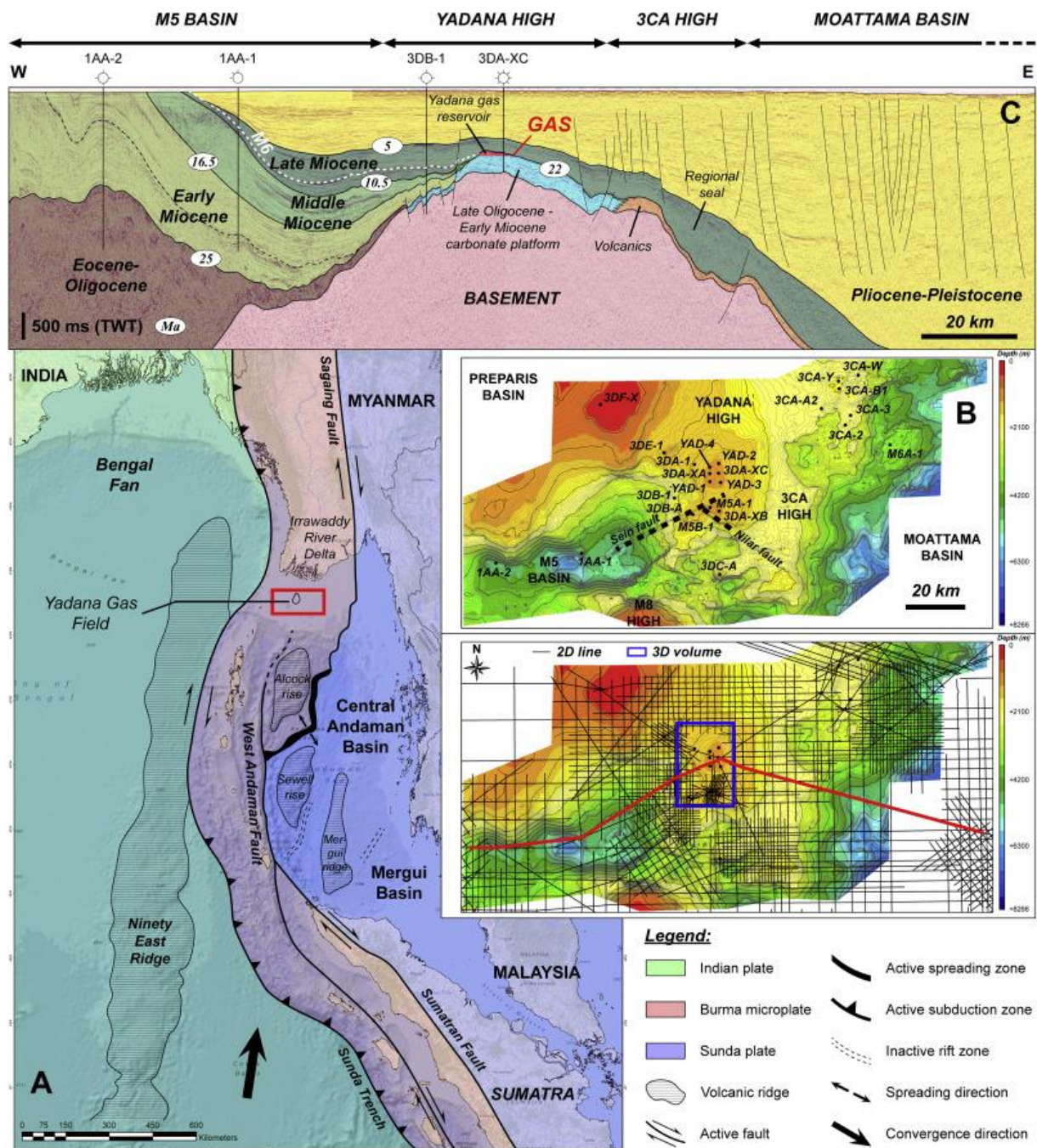


Fig. 2.

(A) Simplified lithostratigraphic column of the Yadana Platform. (B) Three-dimensional view of the top LBL (coherency overlain by depth structure map) in the Yadana Platform. (C) Three-dimensional view of the top UBL (coherency overlain by depth structure map) in the Yadana Platform. (D) Interpreted high-resolution 2D seismic profile (X-X') from 3D seismic data showing the main seismic unconformities of the Yadana Platform corresponding to the top of the different formations. Note the tilting of the GWC in the Yadana Platform. Note as well the presence of another gas field in the overburden (Badamyar Gas Field). LBL = Lower Burman Limestone; UBL = Upper Burman Limestone; GWC = Gas Water Contact; YNP = Yadana North Platform; YSP = Yadana South Platform.

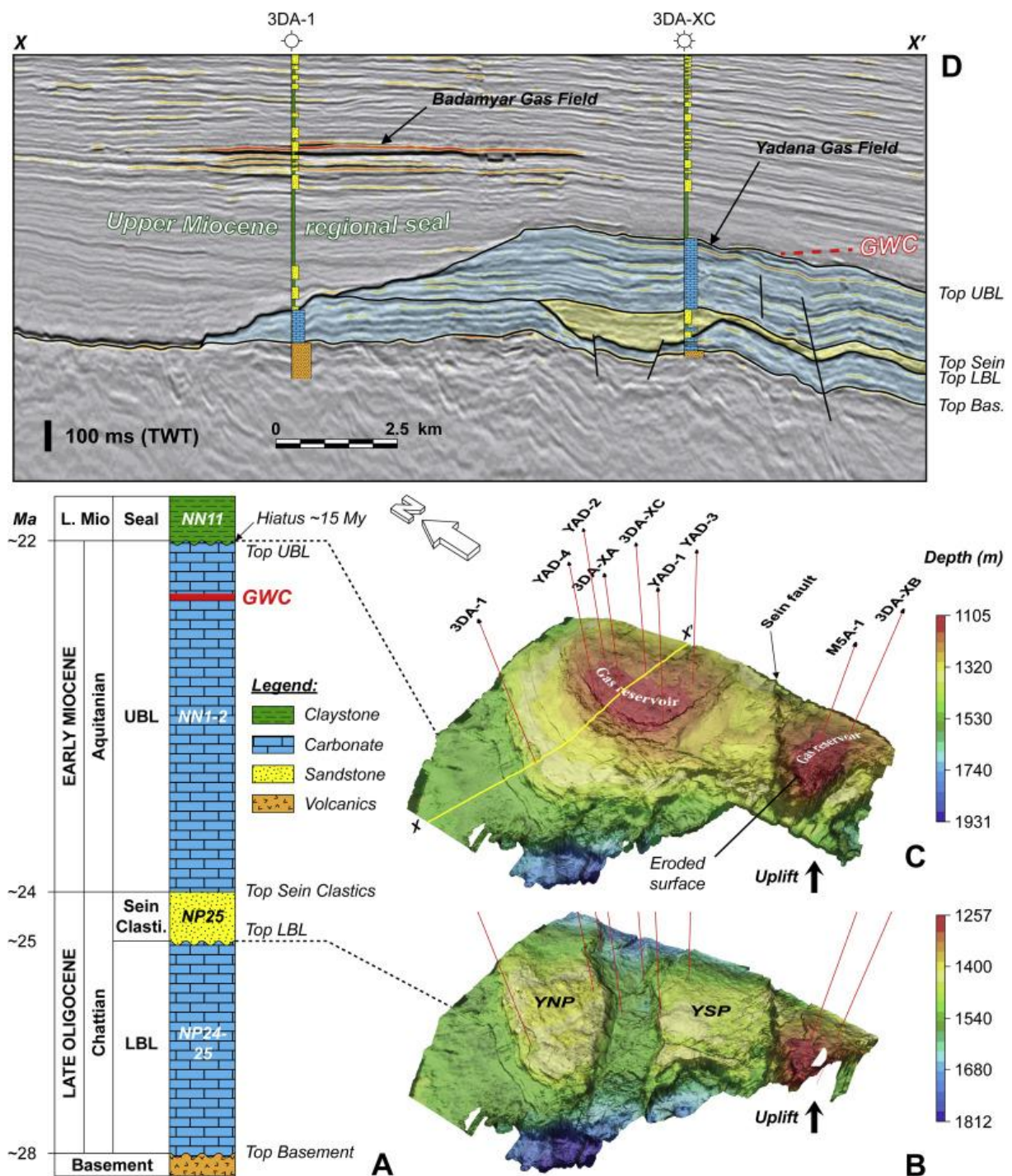


Fig. 3.

Main seismic facies identified on the 2D seismic data with their reflection characteristics (internal geometries, continuity, amplitude, shape). Their identification and interpretation is based on a scheme developed in a similar carbonate setting by [Bachtel et al. \(2004\)](#).

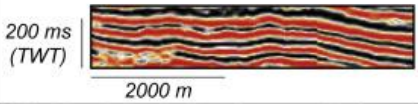
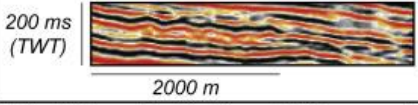
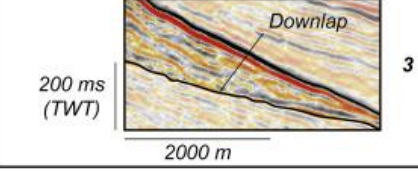
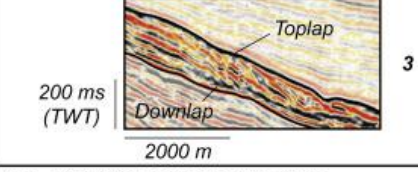
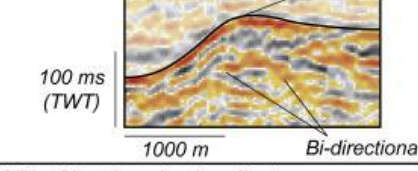
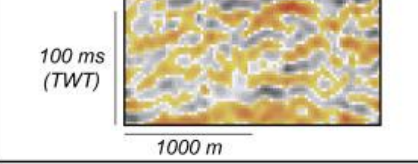
Seismic facies 	Reflection characteristics	Interpretation(s)
<b>SF1 - Parallel seismic reflectors (Basin)</b> 	Sub-horizontal to horizontal parallel reflections Continuous High amplitude	<b>Deep volcanic shelf</b> <i>(Peri-platform carbonates)</i>
<b>SF2 - Parallel seismic reflectors (Platform)</b> 	Wavy to horizontal parallel reflections Continuous High amplitude	<b>Lagoon</b> <i>(Platform rimmed by barrier reef)</i>  <b>Inner-platform</b> <i>(Open platform)</i>
<b>SF3 - High-angle clinofolds (oblique parallel)</b> 	Downlap of lower reflection terminations Oblique parallel clinofolds Semi-continuous to continuous Moderate to high amplitude	<b>Slope</b> <i>(Carbonate shedding)</i>
<b>SF4 - High-angle clinofolds (sigmoid)</b> 	Downlap and toplap of reflection terminations Sigmoidal clinofolds Semi-continuous Moderate to high amplitude	<b>Slope</b> <i>(Carbonate progradation)</i>
<b>SF5 - Mounded seismic reflectors</b> 	Bi-directional downlap of reflection terminations Mound shape (convex-up) Discontinuous to semi-continuous Low to moderate amplitude	<b>Barrier reef</b> <i>(Platform margin)</i>  <b>Patch reef</b> <i>(Platform interior)</i>
<b>SF6 - Chaotic seismic reflectors</b> 	Chaotic to wavy reflections Discontinuous (highly disrupted) Low amplitude	<b>Shoal</b> <i>(Platform margin)</i>  <b>Apron</b> <i>(Platform interior)</i>

Fig. 4.

Un-interpreted (A) and interpreted (B-C) regional 2D seismic profile (A-A'; see location on E) showing the main seismic unconformities (U0-U7), and their correlative conformities, bounding the different seismic sequence (S1-S7). The internal geometries allow characterizing the main seismic facies (see Fig. 3) for each seismic sequence. The small seismic lines corresponds to close-ups showing (from left to right) the leeward side of the Yadana Platform highlighting important progradations; and a bioconstruction located at the top of the seismic sequence S7. The bottom well panel (D) presents the main lithologies of the Late Oligocene - Early Miocene interval. (E) Base seal depth-structure map (bold contours are every 500 m) interpreted from regional 2D seismic data showing the location of the main 2D seismic lines interpreted in this study.

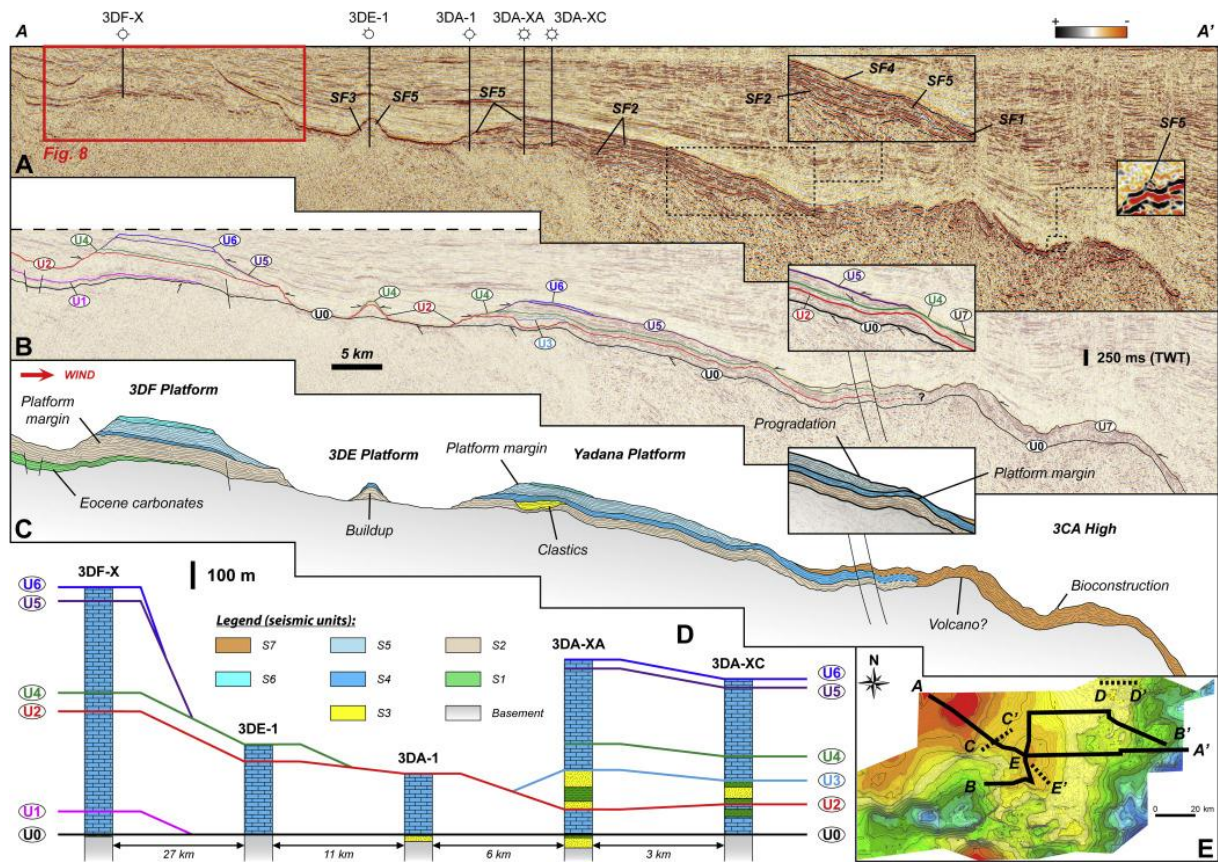


Fig. 5.

Un-interpreted (A) and interpreted (B-C) regional 2D seismic profile (B-B'; see location on Fig. 4e) showing the main seismic unconformities (U0-U7), and their correlative conformities, bounding the different seismic sequences (S1-S7; see legend on Fig. 4). The internal geometries allow characterizing the main seismic facies (see Fig. 3) for each seismic sequence. The small seismic lines correspond to close-ups showing (from left to right) the toe-of-slope debris located on the west part of the Yadana Platform; the onlap of the seismic sequence S7 on the Yadana Platform showing a post-depositional volcanic event; and the chaotic configuration of the M6A-1 well area where some bioconstructions can be identified. The bottom well panel (D) presents the main lithologies of the Late Oligocene - Early Miocene interval.

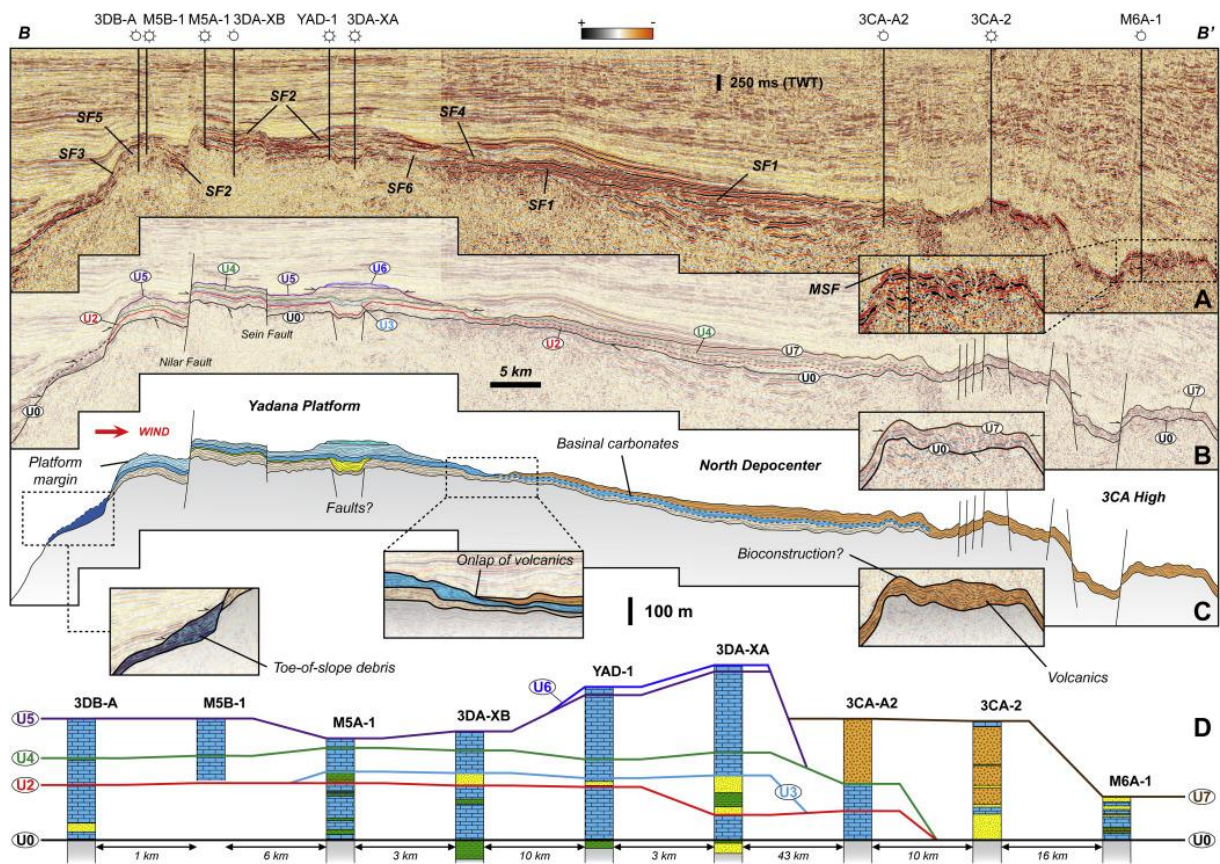


Fig. 6.

Un-interpreted (A) and interpreted (B-C) high-resolution 3D seismic profile (Y-Y'; see location on Fig. 7a) showing the main seismic unconformities (U0-U6), bounding the different seismic sequences (S2-S6; see legend on Fig. 4e) of the Yadana Platform. The internal geometries allow characterizing the main seismic facies (see Fig. 3) for each seismic unit. Close-ups (D and E) highlight respectively the progradations (high-angle clinoforms) of the seismic sequence S3 within the trough and the presence of the seismic facies SF5 in the same sequence.

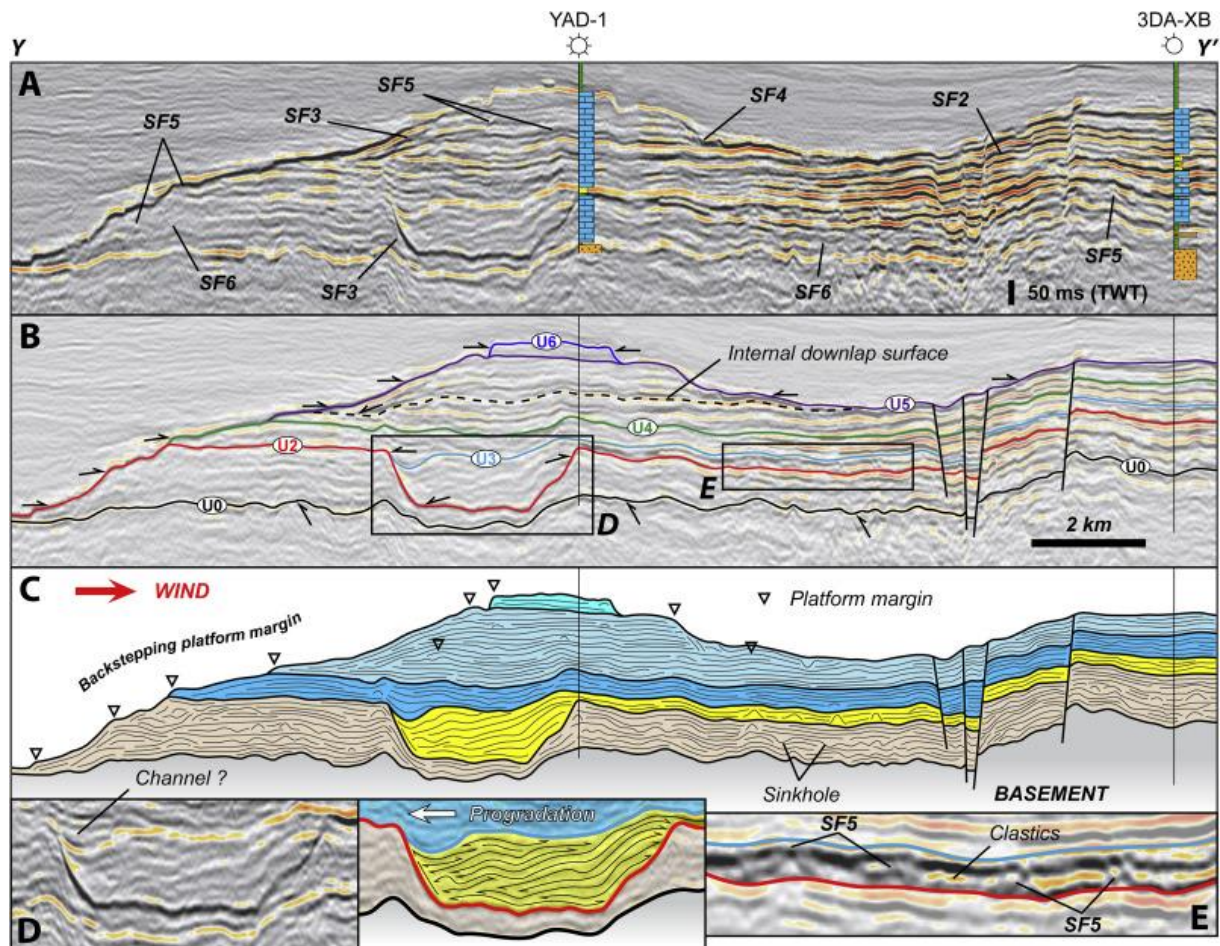


Fig. 7.

2D seismic lines (B to D; see location on A) highlighting the presence of seismic facies SF2 between the platform margin and the 3CA High. Note the presence of the seismic facies SF5 within the same package.

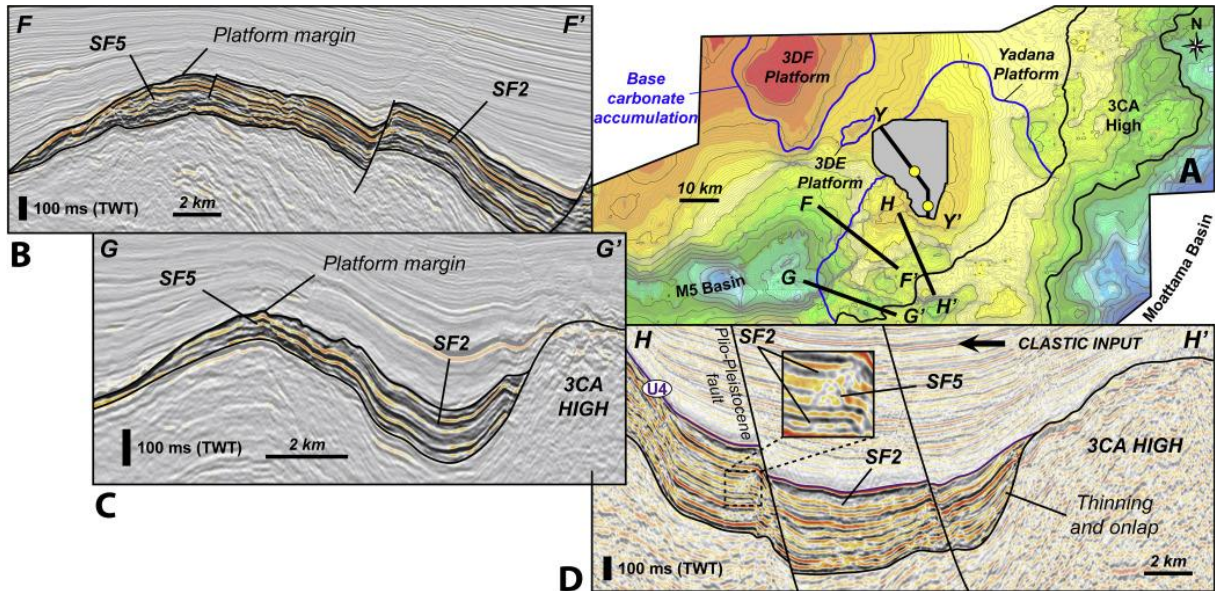


Fig. 8.

Un-interpreted (A) and interpreted (B-D) 2D seismic profiles (close-up from Fig. 4a) showing the main seismic unconformities (U0-U6), bounding the different seismic sequences (S1-S6; see legend on Fig. 4) of the 3DF Platform. The internal geometries allow characterizing the main seismic facies (see Fig. 3) for each seismic sequence and the characterization of the main depositional environments through space and time (see Fig. 13). Note that the fault movement stopped during the seismic sequence S2 but has allowed the creation of internal progradations. Note as well the main erosional truncation along the U2.

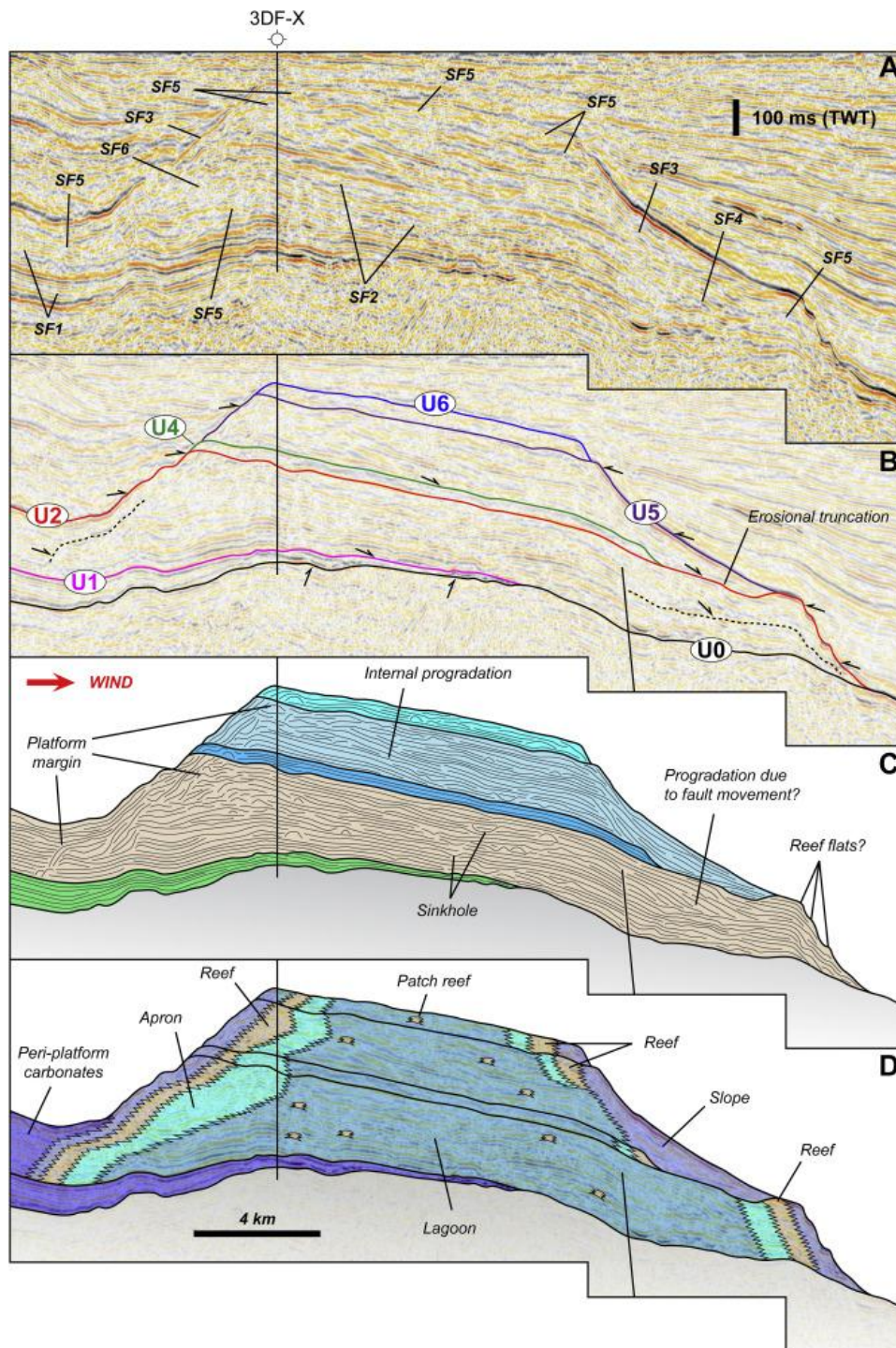


Fig. 9.

Un-interpreted (A) and interpreted (B-C) 2D seismic profiles (see location on Fig. 4e) showing a complete view of the 3DE Platform (C-C'); the presence of lava flows associated with volcanoes in the seismic sequence S7 (D-D'); and a close-up of the north margin of the YSP highlighting a perfect transition between the seismic facies SF5, SF6 and SF2. The main seismic unconformities (U0-U7) are identified, bounding the different seismic sequences (S2-S7; see legend on Fig. 4). The internal geometries allow characterizing the main seismic facies (see Fig. 3) for each seismic sequence.

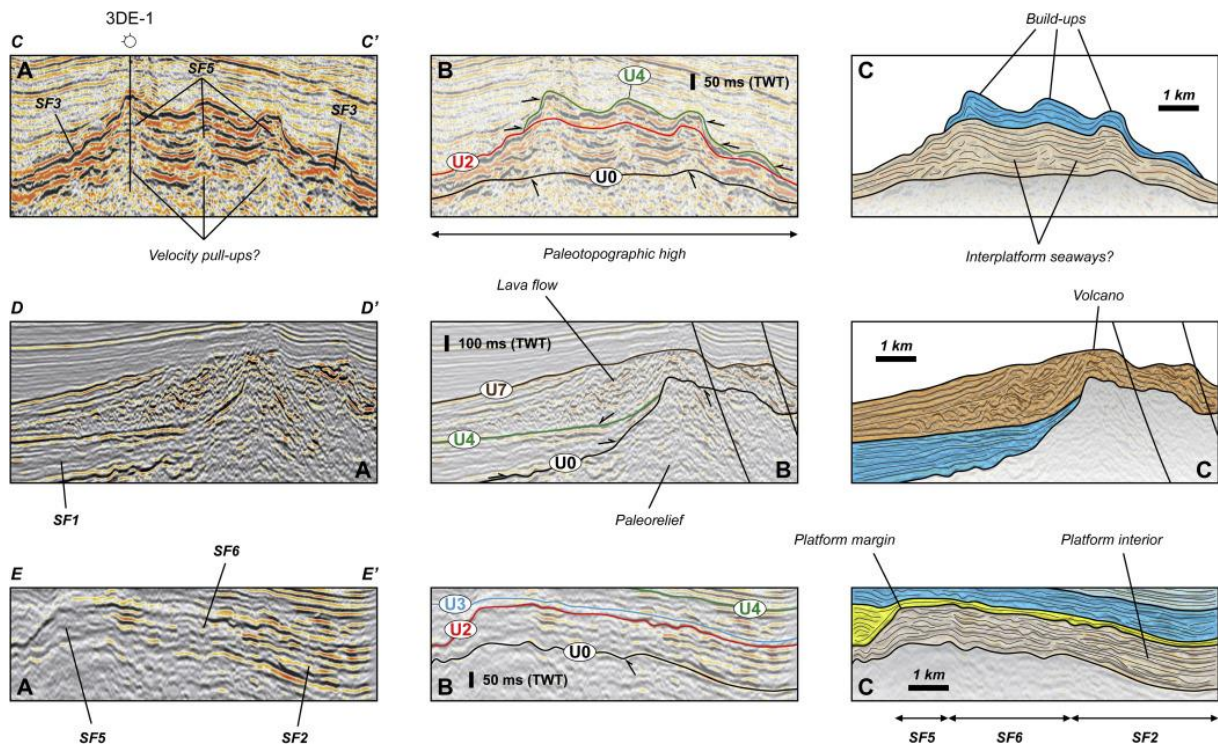


Fig. 10.

(A-C) Respectively coherency attribute map; RMS attribute map; and color-blended (RGB) spectral decomposition attribute map (at 20, 40 and 60 Hz) along the seismic unconformity U2 showing the different geomorphological features observable at the end of the seismic sequence S2 (time window  $\sim 20$  ms TWT). The cross-checking of these attribute maps allows the definition of architectural elements (see [Table 1](#)). Note that the Yadana Platform was first initiated as two platforms (Yadana North Platform and Yadana South Platform) separated by a  $\sim 3$  km interplatform seaway.

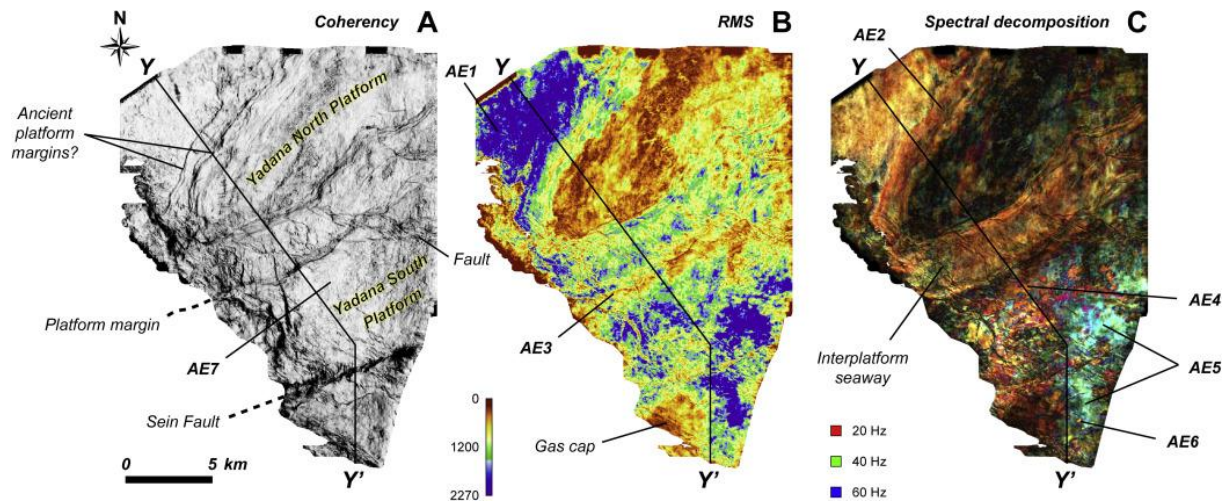


Fig. 11.

(A) Detailed mapping of the architectural elements (see [Table 1](#)) along the seismic unconformity U2 (top seismic sequence S2) showing the main geomorphological features of the Yadana North Platform (YNP) and the Yadana South Platform (YSP). The interpretation highlights a crescent reef barrier on the YNP whereas the YSP shows a more complex organization. (B) Satellite view of a straight seaway between two atolls of the Maldives Archipelago. (C) Color-blended (RGB) spectral decomposition attribute map (at 20, 40 and 60 Hz) of a sinkhole feature (see location of the close-up on A) surrounded by reefs. This configuration reminds the present-day Blue Hole located in the Belize Barrier Reef (D). (E) Satellite view of the windward side of the Glorieuses Archipelago with the interpretation of the main geomorphological features ([Jorry et al., 2016](#)). Source of satellite photos: Google Earth. (For interpretation of the references to colour in this figure legend, the reader is referred to the web version of this article.)

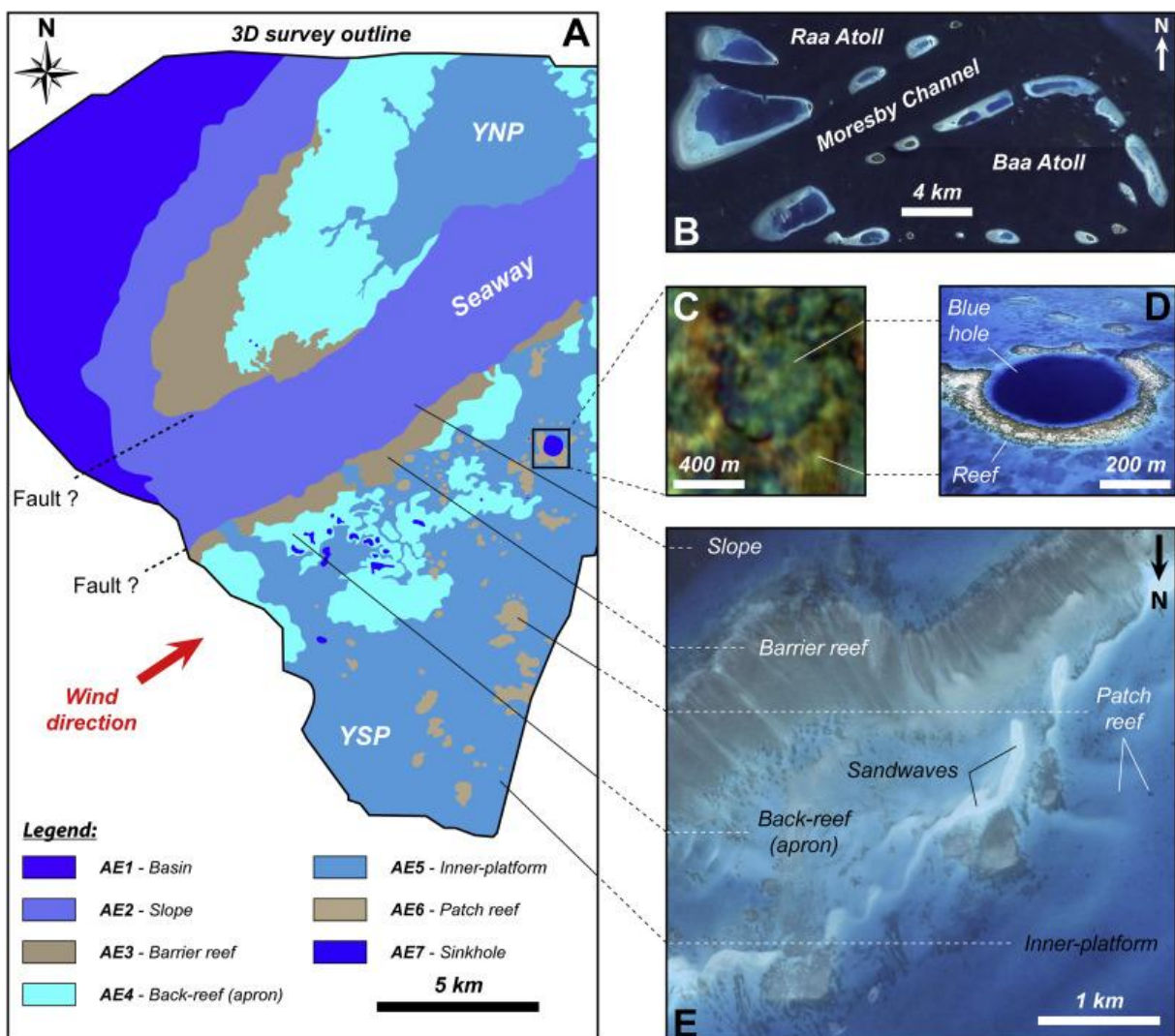


Fig. 12.

(A) Color-blended (RGB) spectral decomposition attribute map (at 20, 40 and 60 Hz) along the seismic unconformity U6 showing the different geomorphological features observable at the end of the seismic sequence S6. (B) Detailed mapping of the architectural elements (see [Table 1](#)) along the seismic unconformity U6 (top seismic sequence S6) showing the main geomorphological features of the Yadana Platform. The interpretation highlights a reef barrier/apron/lagoon succession. (C) Satellite view of a reef platform located in the west part of the Raa Atoll in the Maldives Archipelago. The distribution of the platform domains is equivalent to the ones observed along the seismic unconformity U6. (D) Close-up showing a sinkhole on the seismic unconformity U6. (E) 2D seismic profile showing a deep sinkhole at the top of the Yadana Platform (S-S'; see location on D). (F) Satellite view of a present-day analogue of an intra-reef flat depression located on the Glorieuses Archipelago, interpreted as a sinkhole formed during the last glacial maximum ([Jorry et al., 2016](#)). Source of satellite photos: Google Earth.

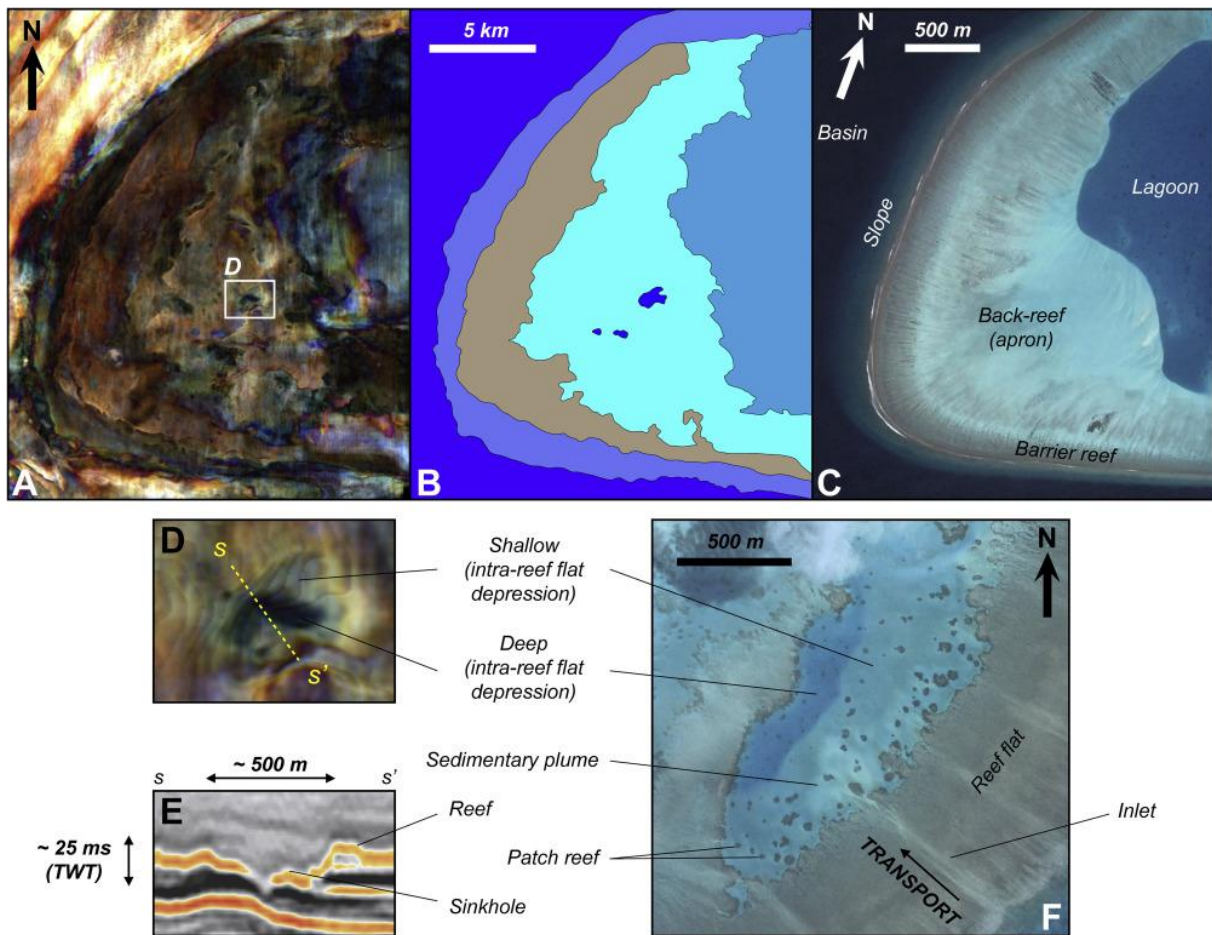


Fig. 13.

3D conceptual depositional model showing the interpretation of the main depositional environments from the seismic facies and architectural elements analysis.

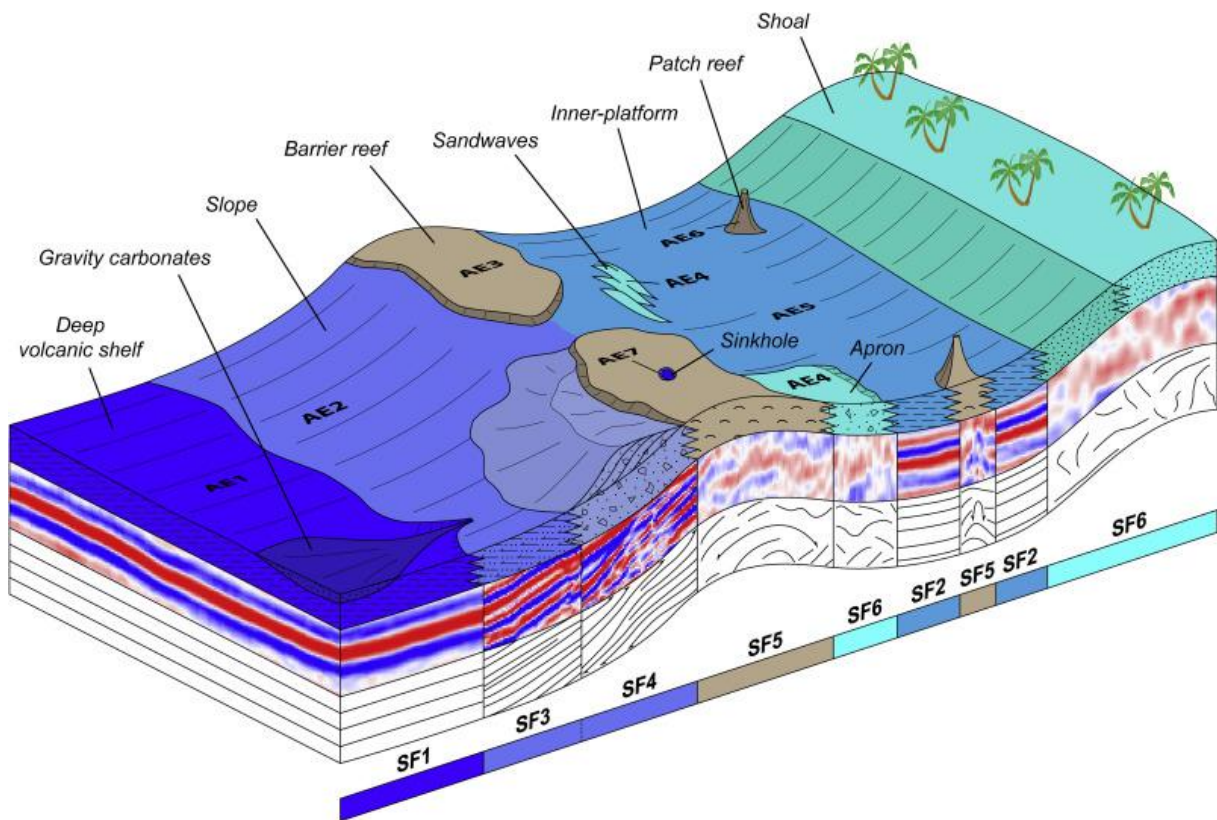


Fig. 14.

Paleogeographical maps interpreted for each seismic sequence (seismic sequences S2 to S7). Note the presence of a paleorelief (3CA) during the entire carbonate depositional history. The carbonate production was initiated during the Chattian on four carbonate platforms: 3DF, 3DE, YNP and YSP. The 3DE Platform was initiated as three isolated carbonate buildups. A period of emersion occurred during the Late Chattian before the carbonate production started again at the beginning of the Aquitanian. During this period, the 3DE Platform is drowned and km-scale backstepping stages occurred on the Yadana Platform, which went from a rimmed setting to an isolated setting. The 3DF Platform presents an atoll configuration during this entire period; whereas the Yadana Platform displays an open-marine configuration once isolated. After a period of volcanic activity, fringing carbonates are developed during the Burdigalian. The cross section at the bottom synthesizes the main depositional environments and provides a legend for the different colors used.

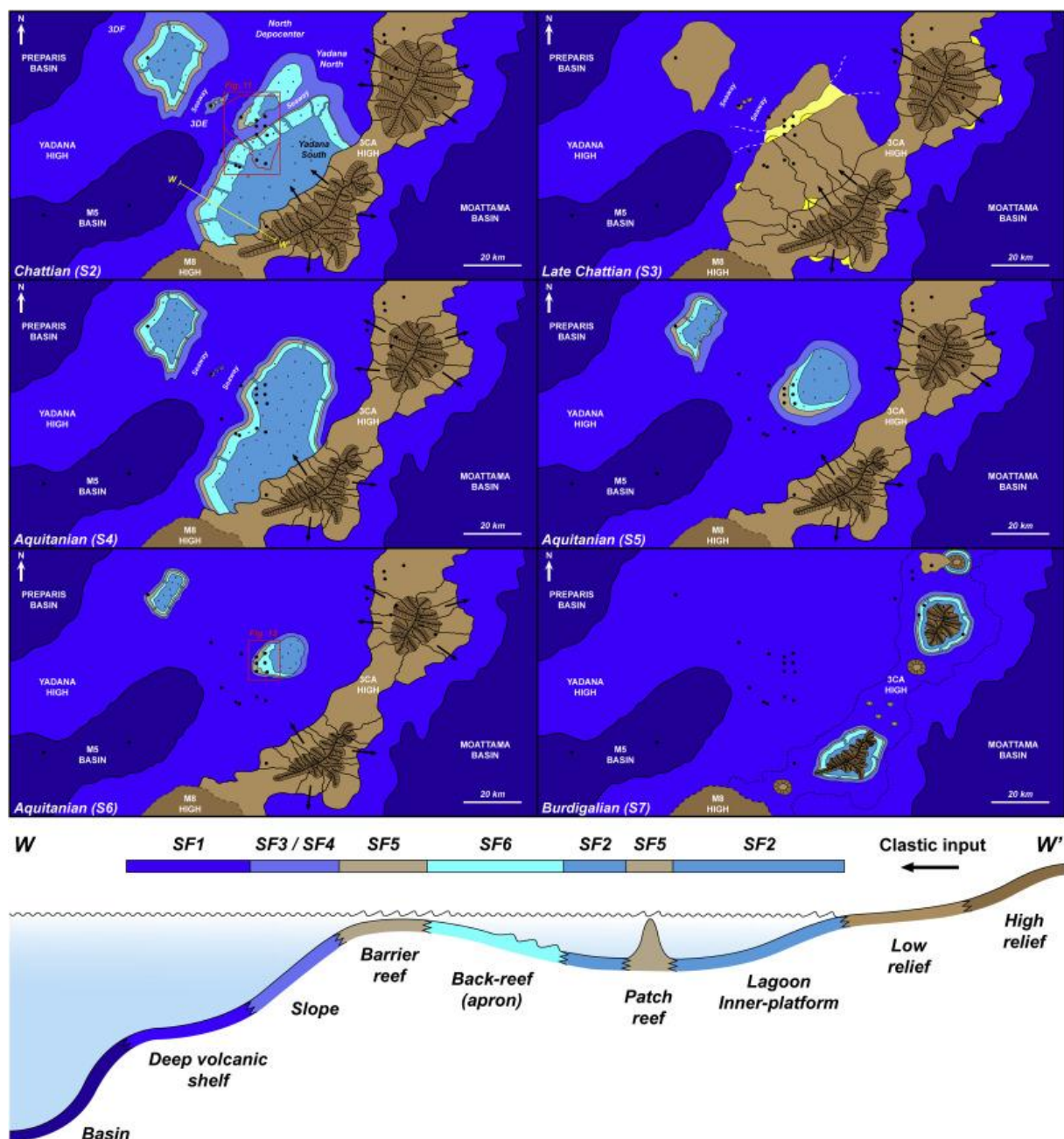


Fig. 15.

Paleogeographical evolution of the carbonate platforms during the Late Oligocene - Early Miocene in the Yadana area in three main stages. (A) A first phase (Chattian) of carbonate aggradation through a transgressive cycle (2nd order). Note the isolated context of the platforms except the YSP, rimmed to the 3CA paleorelief, bringing clastic sediments into the lagoon through proximal and distal plumes. (B) A second phase (Late Chattian) of sea-level fall, leading to the emersion of the platforms (sinkholes development) and the creation of fluvial systems on the YSP, allowing the deposition of clastic sediments in the interplatform seaway. (C) A third phase (Aquitanian) of carbonate aggradation through a rapid transgressive cycle (2nd order) leading to the drowning of the 3DE Platform and the creation of km-scale backstepping features on the Yadana and 3DF platforms. The volcanism on the 3CA High is inferred to appear during the Aquitanian, linked with the later development of fringing carbonates during the Burdigalian.

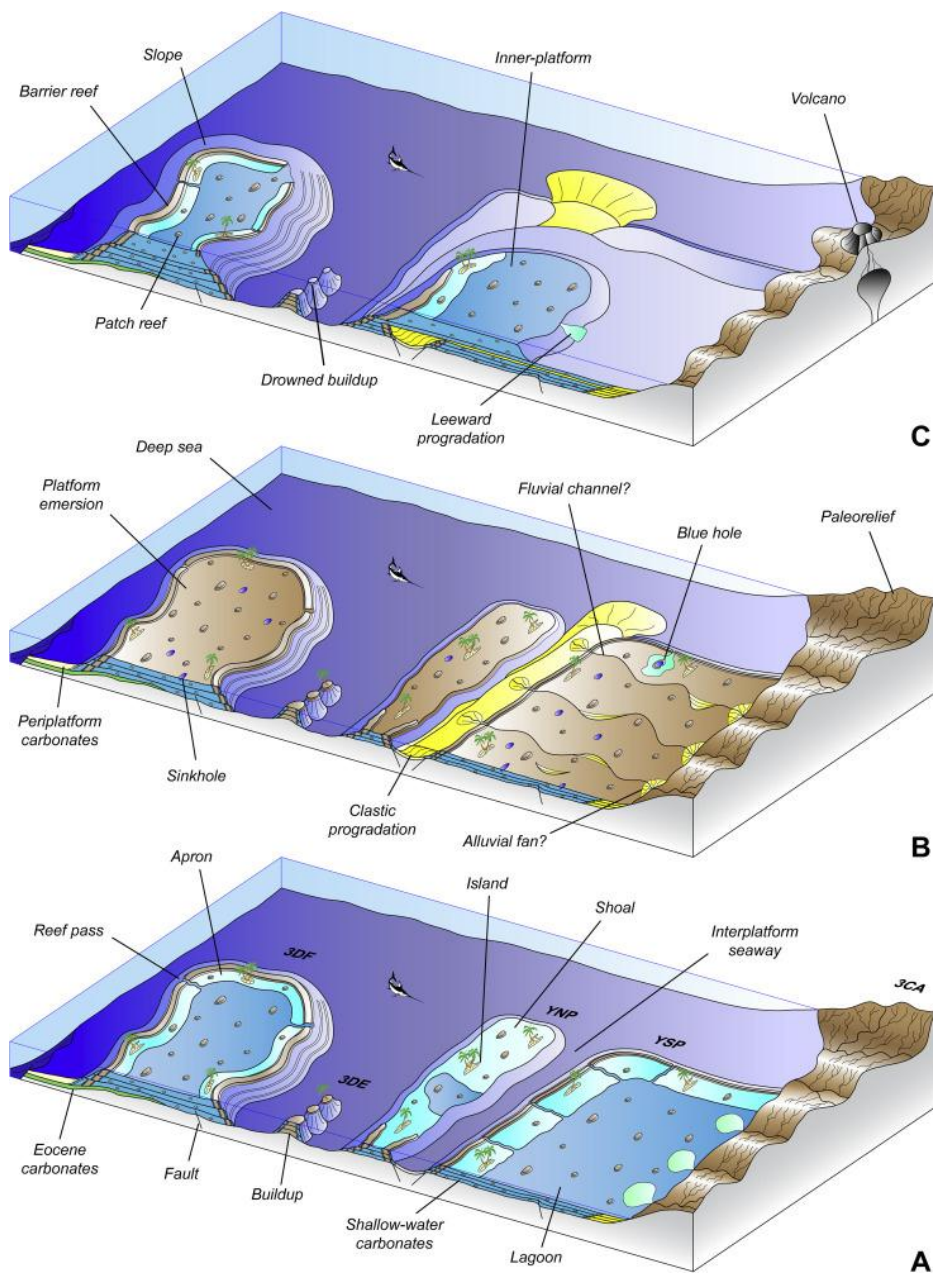


Fig. 16.

(A) Scheme of the tilting ridge hypothesis explaining the higher accumulation of shallow-water carbonates on the 3DF Platform and the creation of the 3CA paleorelief allowing the attached setting of the Yadana Platform during the first sequences of development (seismic sequences S2 to S4). (B) Satellite view of the Central Indian Ocean with location of the Maldives and the 90°E Ridge. Note that during the Late Oligocene - Early Miocene times, both the Maldives and the carbonate platforms lying on the Yadana Ridge were located in the Indian Ocean. (C) Interpreted cross-section through the Maldives Archipelago showing the carbonate strata from the Eocene to the Aquitanian (after [Belopolsky and Droxler, 2003](#)). (D) Interpreted cross-section through the Yadana area showing the 3DF Platform, the 3DE Platform and the Yadana Platform. This interpretation has been realized following a flattened 2D seismic line. Note the tilting of the ridge toward the west from the beginning of the carbonate depositional history highlighted by the onlap of the Eocene carbonate toward the east. Note as well the similarities (e.g. geomorphology) with the carbonate platforms of the Maldives Archipelago (C). Source of satellite photos: Google Earth.

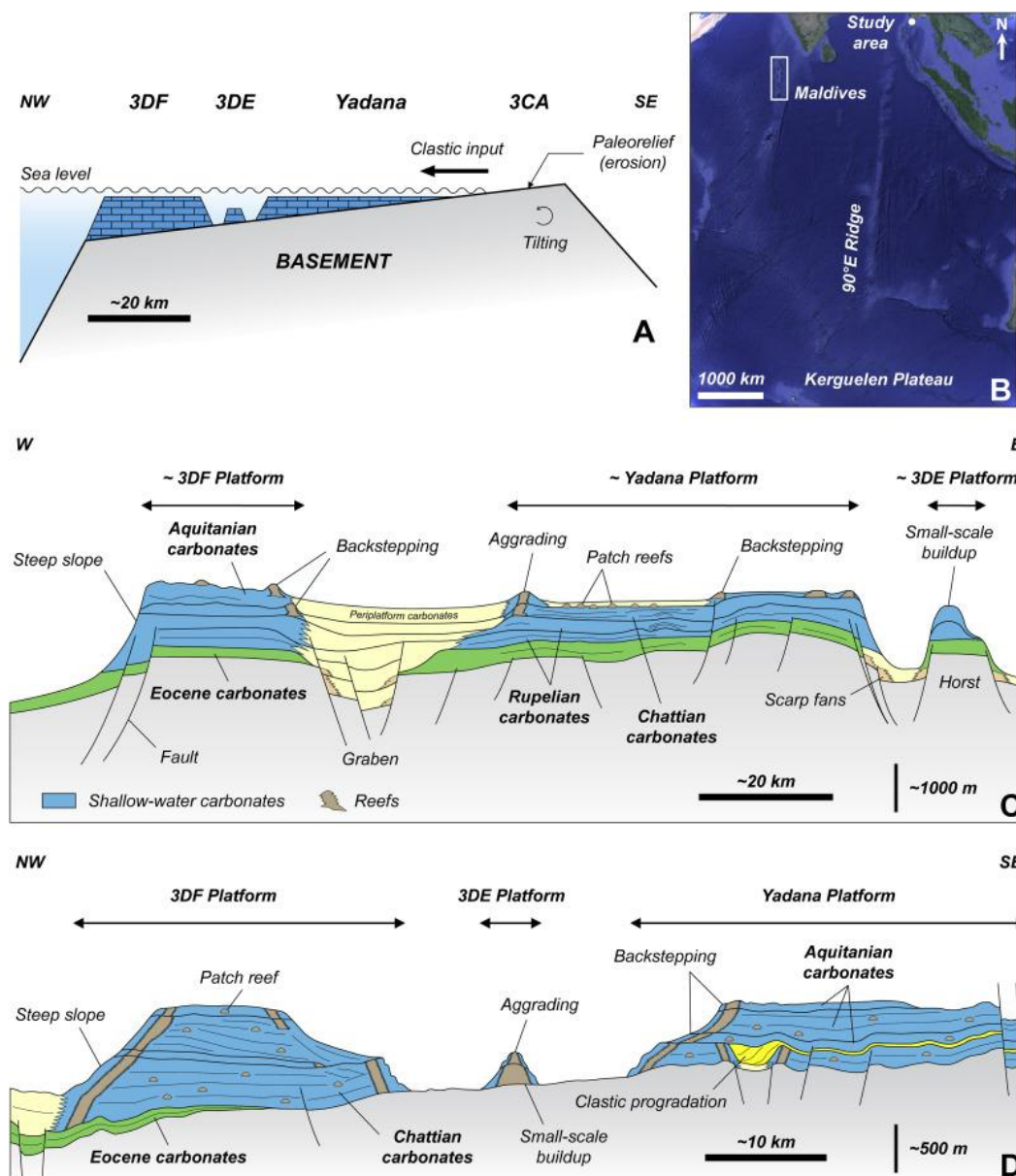


Table 1.

Identification criteria of the architectural elements (AE) from the cross-checking of coherency, amplitude and spectral decomposition maps (see Fig. 10). The interpretation is associated with the main seismic facies identified in Fig. 3. H = High; M = Medium; L = Low.

AE	Coherency	Amplitude	Frequency	Shape	Seismic facies	Interpretation
1	/	H	L	/	SF1	Deep volcanic shelf
2	Along major discontinuity (basinward side)	M	L	/	SF3	Slope (Fore-reef)
3	Along major discontinuity (platform interior side)	L	L	/	SF5	Barrier reef
4	/	L/M	L/M	/	SF6	Apron/Shoal
5	/	H	H	/	SF2	Lagoon
6	Sub-circular discontinuity	L	L	Sub-circular	SF3	Patch reef
7	Sub-circular discontinuity	H	M/H	Sub-circular	SF6	Sinkhole